Single Molecule Tracking in Confined Geometries

by

Mustafa Yorulmaz

A Thesis Submitted to the

Graduate School of Engineering

in Partial Fulfillment of the Requirements for

the Degree of

Master of Science

in

Materials Science and Engineering

Koc University

August 2009

Koc University

Graduate School of Sciences and Engineering

This is to certify that I have examined this copy of a master's thesis by
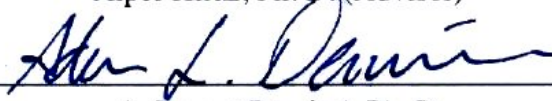
Mustafa Yorulmaz

and have found that it is complete and satisfactory in all respects,

and that any and all revisions required by the final

examining committee have been made.

Committee Members:

_____
Alper Kiraz, Ph. D. (Advisor)

_____
A. Levent Demirel, Ph. D.

_____
Alphan Sennaroğlu, Ph. D.

Date: August 6, 2009

ii

ABSTRACT

Single molecule experiments were performed utilizing total internal reflection fluorescence microscopy technique at room temperature for understanding diffusion dynamics of single molecules in confined geometries of diblock copolymer thin films. The characteristic behavior of single molecules such as blinking and photobleaching were first shown indicating the observation of real dyes rather than some scattering. Then, ~1.5 nm resolution of our experimental setup in positioning fluorescent dyes was shown which allowed us to study the dynamics of single molecules inside the obtained confined geometries (channel diameters ~12-30 nm) and to analyze the surface morphology of different block copolymer thin films. For this purpose, terrylene and rhodamine B dye molecules were used and embedded in PS, PMMA and three different molecular weight PB-PEO diblock copolymers. Rhodamine B and terrylene dye molecules were incorporated with PMMA and PS polymers for understanding and observation of characteristic behavior of single molecules, respectively. They were also utilized for the determination of resolution of our experimental setup in positioning single dye molecules. The usage of terrylene molecules in PB-PEO diblock copolymer samples was for studying the confined diffusion of single molecules.

After spun-casting the thin films which were prepared by using PB-PEO diblock copolymer solutions including terrylene molecules, they were annealed to obtain better intended morphology. By this way, cylindrical channels of PB inside PEO crystalline matrix and 2-dimensional layer of PB at air film interface on top of PEO layer were obtained for providing 1- and 2-dimensional diffusion of terrylene dyes. After that, the trajectories of diffusion single molecules were obtained and analyzed. In this manner, the motion of terrylene probe molecules in confined PB channels having different channel diameter of two asymmetric PB-PEO diblock copolymers and the normal diffusion of terrylene dyes in 2-dimensional PB layer of symmetric PB-PEO diblock copolymer were investigated.

The distribution of 1-dimensional diffusion coefficients were found to have narrower distribution compared to 2-dimensional diffusion coefficients in PB. In addition to normal diffusion of terrylene dyes, directed motion of them was also observed through the trajectories of some single molecules and their analysis where mean square displacement had parabolic time dependence. The origin of this behavior was explained by the presence of some defects in channel formations, i.e. change in local density inside the channel due to local variations in the PB channel width. Furthermore, effects of non-uniformities and heterogeneities in channels on motion of single molecule were studied demonstrating the sensitivity of single molecule tracking in characterizing self-assembled block copolymer morphologies where the trajectories of single molecules were well correlated with AFM and SEM results.

ÖZET

Tek moleküllerin ikili blok kopolimerlerin kullanılması ile elde edilen çevrelenmiş geometrilerdeki yayınım dinamiklerini anlamak için oda sıcaklığında tam içten yansımalı ışıma mikroskoplaması tekniği kullanılarak tek molekül deneyleri yapıldı. Öncelikle, tek moleküllerde görülen ışımanın yanıp sönmesi ve tümüyle sönmesi (görüntü şiddetinin bir basamakta gürültü seviyesine inmesi) fenonmenleri gözlenen ışımaların çeşitli saçılmalardan ziyade gerçekten tek moleküllerden geldiğini bildirmek amacıyla gösterildi. Ayrıca, moleküllerin çevrelenmiş geometrilerdeki (kanal çapları ~12-30 nm) yayınımlarının izlenmesinin ve elde edilen ikili blok kopolimerlerden elde edilen örneklerde oluşan yüzey şekil özelliklerinin incelenmesinin kullanılan deney düzeneği ile mümkün olduğunu göstermek için moleküllerin konumlandırılmasında ~1.5 nm'lik hassasiyete ulaşıldığı gösterildi. Bu amaçlar doğrultusunda, terrylene ve rhodamine B molekülleri kullanıldı ve bu moleküller PS, PMMA polimerleri ve farklı molekül ağırlıklarında üç ayrı PB-PEO ikili blok kopolimerleri içlerine gömüldü. Sırasıyla rhodamine B ve terrylene molekülleri, tek moleküllerin (ışıyan tek boya molekülleri) karakteristik özelliklerini anlamak ve incelemek için PMMA ve PS polimerleri içerisinde kullanıldı. Bu moleküller bahsedilen polimerler içerisinde ayrıca deneysel düzeneğin tek moleküllerin konumlandırılmasındaki çözünürlüğünün hesaplanmasında da kullanıldı. Terrylene molekülleri ayrıca, PB-PEO ikili blok kopolimer örnekleri içerisinde moleküllerin çevrelenmiş geometrilerdeki difüzyonlarının incelenmesi için kullanıldı.

Terrylene moleküllerini içeren PB-PEO ikili blok kopolimer çözeltilerinin spin kaplanmasıyla elde edilen ince filmler, yüzey üzerinde önceden belirlenmiş şekil özelliklerini daha düzgün bir şekilde elde edebilmek için tavlandı. Bu sayede, terrylene moleküllerinin 1- ve 2- boyutlu yayınım yapmalarını sağlayacak PEO kristali içerisinde silindirik PB kanalları ve hava-film ara yüzeyinde PEO katmanı üzerinde 2- boyutlu PB katmanı elde edildi. Bunun

sağlanmasından sonra, bu kanallar içerisinde ve katman yüzeyinde yayınım yapan moleküllerin izledikleri yollar çıkarıldı ve analiz edildi. Moleküllerin izledikleri yol bilgilerinin kullanılmasıyla yapılan incelemelerde, iki farklı molekül ağırlığındaki asimetrik PB-PEO ikili blok kopolimerleri yüzeyinde oluşan iki farklı genişlikte elde edilen PB kanallarında 1-boyutlu yayınım gösteren ve simetrik PB-PEO ikili blok kopolimerinden elde edilen 2-boyutlu PB katmanında 2-boyutlu yayınım yapan terrylene molekülleri gözlendi.

1-boyutlu yayınım katsayılarının dağılımının 2-boyutlu yayınım katsayılarının dağılımından beklendiği gibi daha dar olduğu bulundu. Terrylene moleküllerinin normal yayınımları dışında ortalama karesel yerdeğişimi ile adım aralığı arasında parabolik ilişki gözlemlenen kanallar içerisinde yayınım yapan ve belli bir yönde akışa maruz kalan moleküller de moleküllerin izledikleri yollar ve bunların analiz edilmesiyle gözlendi. Bu tip bir harekete kanal yapılanması sırasında oluşan bozuklukların sebep olabileceği açıklandı. Şöyleki, PB kanal genişliklerinin bölgesel farklılıkları kanal içerisinde bölgesel yoğunluk değişimiyle sonuçlanabilir ve bu tarz bir hareketin gözlenmesine sebep olabilir. Bunlara ek olarak tek molekül izlenmesi yönteminin kendi kendine yapılanan blok kopolimer yüzey özelliklerinin karakterizasyonundaki hassasiyeti, kanal içerisinde bulunan düzensizlik ve heterojenliklerin molekülün hareketindeki etkileri nin incelenmesiyle vurgulandı. Bunların dışında elde edilen veriler AKM ve TEM sonuçları ile karşılaştırıldı ve sonuçların çok güzel uyum içerisinde olduğu gözlendi.

ACKNOWLEDGEMENTS

TABLE OF CONTENTS

LIST OF TABLES

LIST OF FIGURES

xiv

NOMENCLATURE

TIRFM	total internal reflection fluorescence microscopy
AFM	atomic force microscopy
SEM	scanning electron microscopy
ϕ	quantum yield (efficiency of a fluorescence process)
k_r	radiative decay rate
k_{nr}	non-radiative decay rate
n	index of refraction
T_{img}	minimal time between two images
T_{exp}	exposure time
T_{read}	readout time
N.A.	numerical aperture
d_{min}	resolvable distance between two points
λ	wavelength
$\mu = (x_0, y_0)$	mean value of the distribution
σ_μ	standard error of the mean (standard positioning error)
N	number of collected photons
a	the pixel size of imaging detector
b	the standard deviation of the background
s_i	the width of the distribution
I_0	maximum intensity
N_x, N_y	number of pixels in x- and y-direction

x_i , y_i x- and y-coordinates

σ_{xy} the standard deviation of the Gaussian

σ_{bg}^2 variance of the background intensity

$\sigma^2\left(I\left(x_i, y_i\right)\right)$ local variance of the signal intensity at the position $\left(x_i, y_i\right)$

MSD   mean square displacement

τ lag time

SNR   signal to noise ratio

Chapter 1

INTRODUCTION

1.1 Overview

Optical studies of single molecules opened a way to investigate the dynamics of local environments in solids, liquids and biological systems. Recently, it was performed at room temperature and it was established that single molecule microscopy is a very powerful method to understand the molecular motion of fluorescent dyes in biological [1-6] and chemical [7-12] processes and material science [13, 14] providing the information which was not accessible by other ensemble methods [15-17], like nuclear magnetic resonance (NMR) [18, 19], fluorescence correlation spectroscopy (FCS) [20, 21], neutron scattering techniques [22], etc. By this way, many applications for single molecule imaging have been found especially in nanotechnology in recent years [23-25].

Translational [22, 26, 27] and rotational diffusion [8, 28] and also translation of single molecules with switchable orientation [29-31] were worked to study the most information about characteristics of host materials. Firstly, single molecule experiments were performed at low temperature. Observation of single molecules at room temperature was possible when new filter and objective technology emerged. This progress made it possible to use the single molecule methods in biological environments without damaging them. For instance, in biology, the detection of fluorescence labeled lipid in motion in a fluid lipid membrane was first shown using conventional epifluorescence microscope indicating the fascinating potential of single molecule studies in bioscience [27]. In a recent work, it was

also shown that it is possible to visualize the infection pathway of single viruses labeled with one fluorescent dye in living cells in real time [3].

As single molecule fluorescence microscopy provides the dynamic information of diffusing probe molecules in range of the nanometer scale [4, 32] the most information about characteristics of host structure can be defined by exploring the molecular movement [20]. For instance, in chemistry, single molecule fluorescence microscopy technique was used to monitor the catalytic processes on surfaces providing a better understanding with its high sensitivity down to single molecule than the other methods like transmission electron microscopy (TEM) and scanning tunneling microscopy (STM) limited by the need for low pressure conditions and conductive surfaces, respectively [13]. It was also used for the exploration of the nanosturctured channel systems [11, 33, 34] providing a better understanding about the heterogeneities of the system. In all of this type of experiments, probe molecules such as individual fluorescent dyes are embedded or attached to the system for exploration.

Understanding the dynamics of single molecules in confined spaces of diblock copolymers is what we are interested in this field of study. So, giving the general information and recent work of this type of study would be helpful to create a sense what is newly done in our experiments.

1.2 Diffusion in Confined Geometries

Diffusive transport of particles occurs through the nature of physical and chemical reactions. When there are configurations like walls or constrictions confining the particle into the geometry of interest, the transport of particles and their localization is affected. So, the diffusion of single particles in nano-scales was studied regarding the Brownian motion and other effects that might lead the molecules to make normal 1-dimensional diffusion or to possess different modes of motion such as corralled or directed diffusion [35, 36]

It was shown how single molecules can be utilized as nanoscale probes to map out different topologies using fluorescent molecules as guests in several host structures [34] through the observation of single molecule diffusion. It was also possible to determine the 3D orientation for probing the confined fields by comparing the simulated and measured image patterns of single molecules showing the use of single molecules in determination spatial distributions of confined optical fields [8, 28]. There are also other works presenting the combination of both these detections [29, 30]. For instance, single TDI molecules were incorporated into the hexagonal mesoporous films and detailed analysis of diffusional and orientational behavior of single TDI molecules diffusing in CTAB-templated pores were made to get the direct information about the influence of local environment on the guest molecule and by this way about the topology [31]. In the light of this evidence, we understand that considerable efforts were put for understanding the dynamics of single molecules in a variety of host systems including mesoporous materials [30, 33, 34], biological membranes [6], defects in crystals [10], molecular sieves [37] and sol-gel glasses [9].

In this work, we study the diffusion dynamics of single probe molecules in confined geometries provided by the self-assembled ordered morphologies of block copolymers to understand the morphology of block copolymer thin films and the effects of local environments on the molecule's movements. Although the potential of block copolymers to form ordered morphologies has been demonstrated in various studies [38], the analysis of single molecules inside them has not been investigated. We describe our purpose in this field in the following section in detail.

1.3 Our Purpose

In our study, we try to understand the diffusion dynamics of single molecules in confined geometries of diblock copolymers and then we describe our investigation on

motion of single probe molecules in these confined spaces and relate the results to the morphology obtained on thin films. For this purpose, the fluorescent dyes were embedded as probes into the thin films of polymer nanostructures having porous and lamellar amorphous structures confined by crystal matrices and dynamics of them were studied using total internal reflection fluorescence microscopy (TIRFM) technique and single molecule tracking tools. A significant amount of data was collected and they were used to obtain an understanding about the morphology of the block-copolymer thin films. Single molecule trajectories were tried to be correlated with the images of host-systems obtained by atomic force microscopy (AFM) and scanning electron microscopy (SEM). Some analysis methods were used highlighting the sensitivity of the motion of single molecules to non-uniformities and heterogeneities in the samples and different modes of motions possessed by different molecules could be shown. Furthermore, the diffusion coefficient of diffusing single molecules in different thin films of diblock copolymers having different molecular weight and topology were measured and compared between each other to understand the differences of single molecule dynamics in different structures.

In order to understand the utilization of single molecule detection tools for the observation of the thin films' morphology, we first needed to have the thin films of diblock copolymer solution including fluorescent dye probes. For this purpose, we chose a specific dye molecule for the specific polymer nanostructure. We, then, prepared our samples and performed single molecule experiments by utilizing TIRFM technique with them. And then we analyzed the results using single molecule methods. All of these procedures are explained in the following chapters in detail.

Before discussing the specific case for our experiments, providing the basic understanding of single molecule experiments would be helpful. This includes the description of previously used host-guest systems, photophysics of single molecules,

conventional experimental setups and their required components. They will be provided in this chapter after describing the thesis outline.

1.4 Thesis Outline

This thesis is subdivided into five chapters including this introductory chapter.

The general overview of dynamic behavior of single molecules for behaving as sensitive reporters inside the host materials and our purpose of performing single molecule experiments is described and typical experimental setups and their components for the observation of them are introduced in Chapter 1.

Chapter 2 covers the description of the materials that were used in our experiments. How we prepared the samples and which geometry we expected to see of them were also discussed with mentioning two characterization techniques; AFM and SEM.

Chapter 3 describes the single molecule techniques specific to our experiments. In the first part, how single molecules were observed using TIRFM is explained showing some results of their characteristic behavior. In the second part, the methods that were used to trace the single molecules and analyze their trajectories are discussed with mentioning typical observed diffusion modes after showing the localization accuracy of our experimental setup in positioning our fluorescent dyes.

Chapter 4 explains the results of single molecule observation inside the PB channels of PB-PEO diblock copolymers. Detailed explanation for a few selected trajectories for every sample correlating the results to the AFM and SEM images is given.

At the end of this thesis, a summary of the performed study and its results with targeted future work are provided in chapter 5.

1.5 Host-Guest Materials

For every fluorescence work, the host-guest materials should be defined first. Host-guest materials are obtained by the incorporation of molecular species to the solid matrix where molecular species are guest and solid matrix is the host. There are numerous functioning examples of these systems which have found a lot of applications such as phosphors [37], sensors [39], waveguides [40], etc. There are numerous ways to form the host-guest material system. For guest species; dye molecules, catalytic complexes, biological active materials, etc. can be utilized whereas host-materials can be polymers, glasses, porous material, etc. In our experiments, we have incorporated fluorescent dyes to polymer networks. The procedure of this incorporation is described in chapter 2 in detail.

1.6 Fluorescence Microscopy

Understanding the fluorescence phenomena is essential for optical microscopy and spectroscopy of single molecule objects. The first thing that is required to be learnt is the principle features and properties of fluorescent molecules.

1.6.1 Fluorescence

The photophysics of single molecules can be described with the help of a simple three level energy diagram (Figure 1.1) (Jablonski diagram) [41]. According to this diagram, the fluorescent dye molecule rests in the singlet S_o state which is the lowest energy state until it is excited by an incoming photon to the singlet S_1 which is the next highest electronic state. For the excitation of the molecule, the incoming photon's energy and polarization has to be suitable.
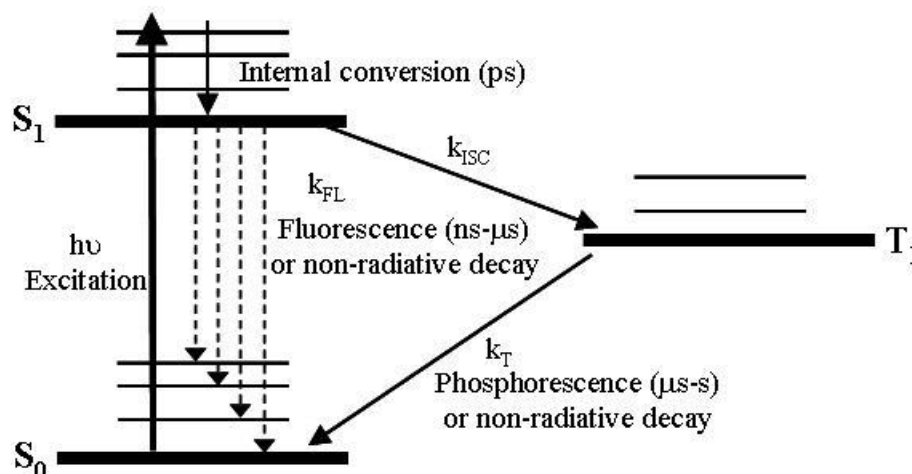
Figure 1.1 Jablonski diagram for describing the photophysics of fluorescent molecules [42].

After the excitation of single molecules from the ground state (S_o), the molecule is first lead to a higher vibrational state in S_1 from where it relaxes to the first excited state (S_1) via internal conversion. From this state, they can return to the ground state (S_o) by emitting a fluorescence photon or by a non-radiative decay. Otherwise, they can possess inter system crossing (ISC) into the triplet state (T_1) from which the excited molecule can return to the ground state (S_o) via another radiationless ISC or by emission of a phosphorescence photon. The first way is the most probable relaxation way of a molecule. The emitted photons in this step make the fluorescence of single molecules. These photons are red shifted due to the Stokes shift. The latter way occurs slower so that the molecules which are kept in triplet state become invisible for a certain time. In an idealized system, the absorption-emission cycle would go on forever. However, this is not the case in real systems due to occurring some irreversible reactions to the molecules which are in the triplet state. This also determines the characteristic behavior of them which are blinking and photobleaching.

Photobleaching is the destruction of fluorescence and it occurs due to some chemical reactions after a certain number of excitation-emission cycles. Photobleaching results in the

final disappearance of the molecule from observation (Figure 1.2b). Blinking is the consecutive on- and off-behavior in the fluorescence of single molecule and it can be attributed to the transition of single molecule to the triplet state which takes more time occuring the fluorescence (Figure 1.2c). You can see an example epiflurescence image of single molecules of DCDHF-6 in a poly(methyl methacrylate) thin film at room temperature (Figure 1.2a), the photobleaching event (Figure 1.2b) and the blinking near 3 seconds (Figure 1.2c) in the following image.
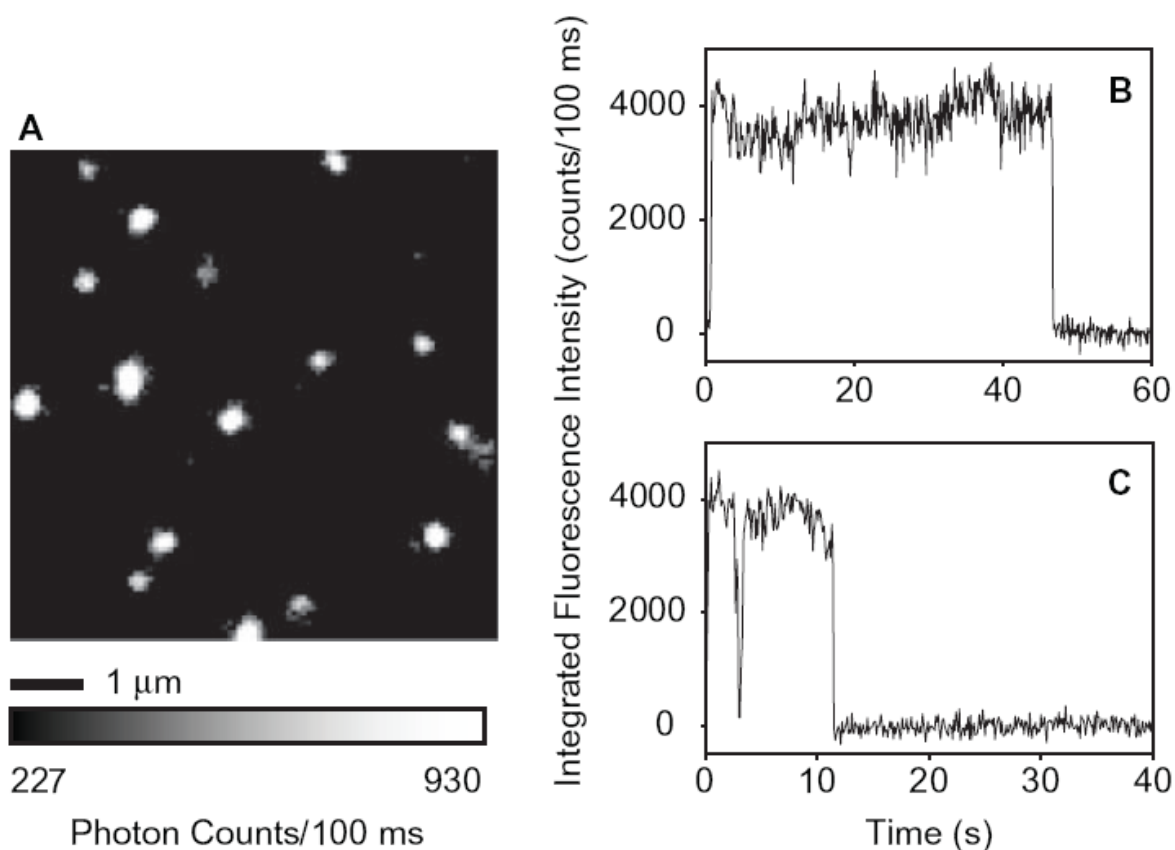
Figure 1.2 Single molecule measurements. a) Single molecule images of DCDHF-6 in PMMA thin film. Time traces of single molecule intensity showing b) photobleaching and c) blinking near 3 seconds and photobleaching near 12 seconds [43].

By this way, single molecule experiments have been performed for different purposes and have found a lot of applications in understanding biological and chemical processes. In those experiments, single molecules are used as local probes for local nano physical and chemical properties of molecular processes in their environments.

For single molecule experiments, there are some important features of fluorescent dyes which make them usable. Firstly, the fluorescence quantum yield is described with the following ratio:

$$\phi = \frac{k_r}{k_r + k_{nr}} \tag{1.1}$$

Where ϕ, k_r and k_{nr} are quantum yield (efficiency of a fluorescence process), radiative decay rate and non-radiative decay rate, respectively.

So, higher k_r of the molecules means better emitter molecules. Furthermore, the fluorescent dye of choice has to be chemically stable for many excitation-emission cycles in such reactive environments as air or water. They also need to be planar and rigid [44].

1.7 Fluorescence Microscopy Techniques for the Observation of Single Molecules

Various single molecule techniques are developed after the first observation of single dye molecule via its absorption [45] or its fluorescence excitation spectrum [14]. The further improvements in design of filters, lenses and the objectives also contributed to this development. For instance, modern interference filters are utilized to separate the fluorescence emission from the background noise and it is possible to collect high amounts of emitted single molecule light by the use of high numerical aperture objectives [42]. Furthermore, with the tools which are available nowadays, detecting single objects even down to nanometer scales becomes trivial. By this way, observation of single molecules is much based on the detection of fluorescent light via fluorescence microscopy techniques.

Here, two different fluorescence microscopy techniques are described which are used to detect and record the fluorescence images for single molecule studies. They are wide-field microscopy technique and confocal microscopy technique which are distinguished according to their detection geometry and type of image recordings. In wide-field microscopy, there is an array detector like a CCD camera to record the images of sample regions of several tens of micrometers in diameter at the same time. In confocal microscopy, fluorescence coming from the small diffraction limited focal volume of the sample can be detected by the use of a photodetector which continues with obtaining the images via moving the sample or scanning the focal spot [44].

In this work, total internal reflection fluorescence microscopy which is a derivative of wide-field microscopy was used for the observation of single molecules since it provides a much higher temporal resolution. So, firstly, the wide-field microscopy is described in detail mentioning the importance of total internal reflection in this type of microscopy and then the working principle of confocal microscopy is introduced in the following sections. Finally, the key experimental components for TIRFM setup are shown. TIRFM setup that we utilized through our experiments is described in chapter 3 in detail.

1.7.1 Wide Field Microscopy

An area of sample is illuminated by a laser beam similar to the conventional white-light microscopy [42]. Fluorescence light of the excited single molecules is separated from the excitation laser by using convenient optical filters. And then, fluorescence is collected by a multi-channel detector such as a CCD camera [42] or an image intensifier [44] (Figure 1.3).
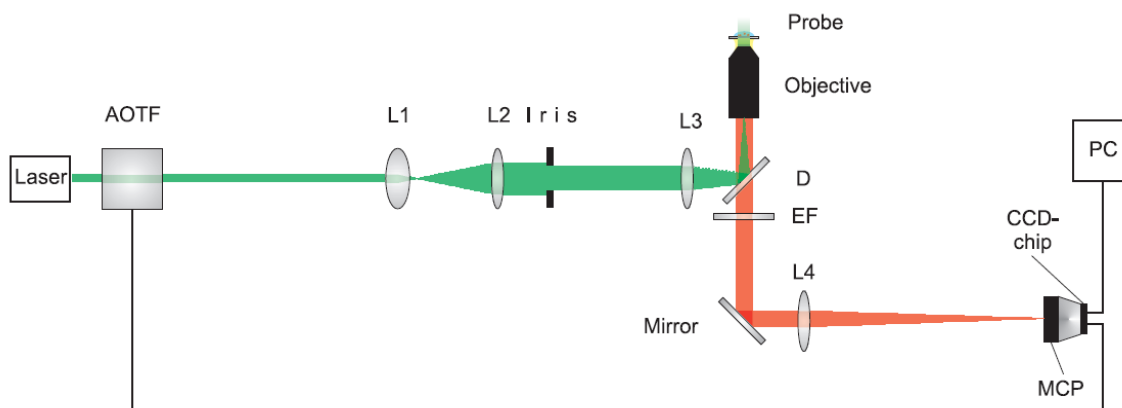
Figure 1.3 Typical wide-field microscopy setup. AOTF: Acousto-optical transmission filter, L: Lens, D: Dichroic mirror, EF: Emission Filter [46].

Background noise is an important issue to consider about in wide field microscopy. This is because during the illumination of the sample and excitation of single molecules, the excitation beam is widened and passes through the entire thickness of the sample and outside the focal plane. So, there occurs emission above and below the imaged plane of the sample. However, this problem can be solved by using the fact that light is totally reflected at large incidence on the surface when it hits a medium which has smaller index of refraction, n. This technique is called objective type total internal reflection fluorescence microscopy which is explained in chapter 3 in detail since we use this technique for the observation of single molecules through our experiments.

Since the area detectors are so much important for every wide-field methods, some information about the working principle of CCD cameras which are used for single molecule experiments is given in the following section.

1.7.1.1 CCD Technology for Single Molecule Experiments

Charged Coupled Devices (CCDs) are image sensors which provide detection of low-light with high signal to noise ratios. CCD chips consist of an array of silicon diode photosensors, the photoactive region, which is connected to charge storage region. When light hits to the photosensor, the electric charge is created which is equivalent with the intensity of light. The quantity of accumulated electric charges is determined by the intensity of light hit and it is read-out by an amplifier. By this way, electric charge is converted into voltage. This conversion is performed row by row of the array; the charges of each row are amplified, coupled, and moves down and out and the successive row follow in turn as illustrated in figure 1.4
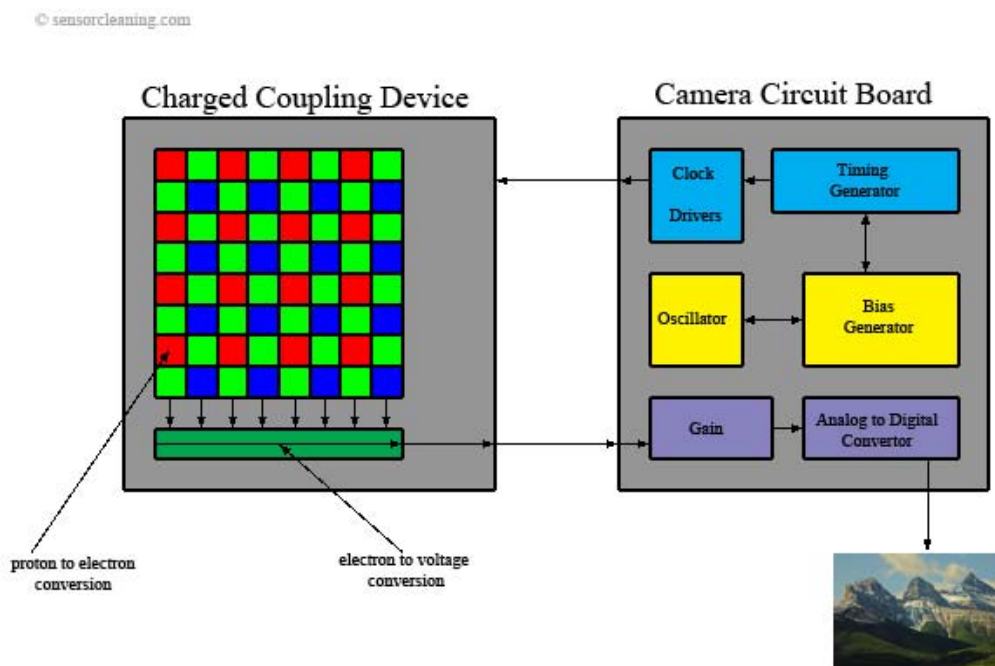
Figure 1.4 Illustration of CCDs operation principle [47].

The temporal resolution of the measurement is given by the minimal time T_{img} between two images which is determined by the exposure time T_{exp} and the readout time T_{read} of the CCD.

In modern CCDs, the sensor part is divided into two sub-regions; the image section and the store section. The store section is shielded from light and as the image section is exposed for about T_{exp}, the charges are transferred from image section to store section to be read out there line (row) by line (row). By this way, as the time for the shift of the charges from image section to the store section exceeds the read out time, the read out time is reduced to the shift time as long as T_{exp} is larger than the time needed to read out the store section [42].

In an EMCCD chip, everything is same with normal CCD chip except the additional on-chip signal amplification. The subsequent amplifying stages make it possible to detect the weak signals, like single-molecule fluorescence. This is achieved as the electronic signal is amplified before it is read out at the output node with the additional multiplication register which increases the sensitivity of the device.

In the light of this evidence, we used Hamamatsu Image EMCCD camera for the detection of single fluorescent dye molecules during our experiments.

1.7.2 Confocal Microscopy

Achievable smallest diffraction limited point of the sample is illuminated and the fluorescence can be imaged by the use of a point detector in this microscopy method. It is possible to record 3-dimensional image by moving the sample in 3-dimensions. A diaphragm of a pinhole is utilized to ensure that the recorded fluorescence is only coming from the focus. By this way, the resolution in the optical z-axis is increased since the out of focus light is blocked. In order to obtain the full image of the area of interest on the sample, the excitation focus or the sample is moved point by point [42]. Scanning the area of

interest on the sample can be done by tilting the mirrors which would move the focus (beam scanning) or by using a piezo-electric transducer which would move the sample itself (sample scanning). In this type of microscopy technique, the signal intensity is recorded as a function of position of the sample [44]. However, this technique becomes also useful to determine the orientation of the molecule in the observation plane by introducing a polarizer into the excitation and detection pathway [8, 29, 30]. Below, schematic of an example confocal microscopy setup is shown (Figure 1.5)
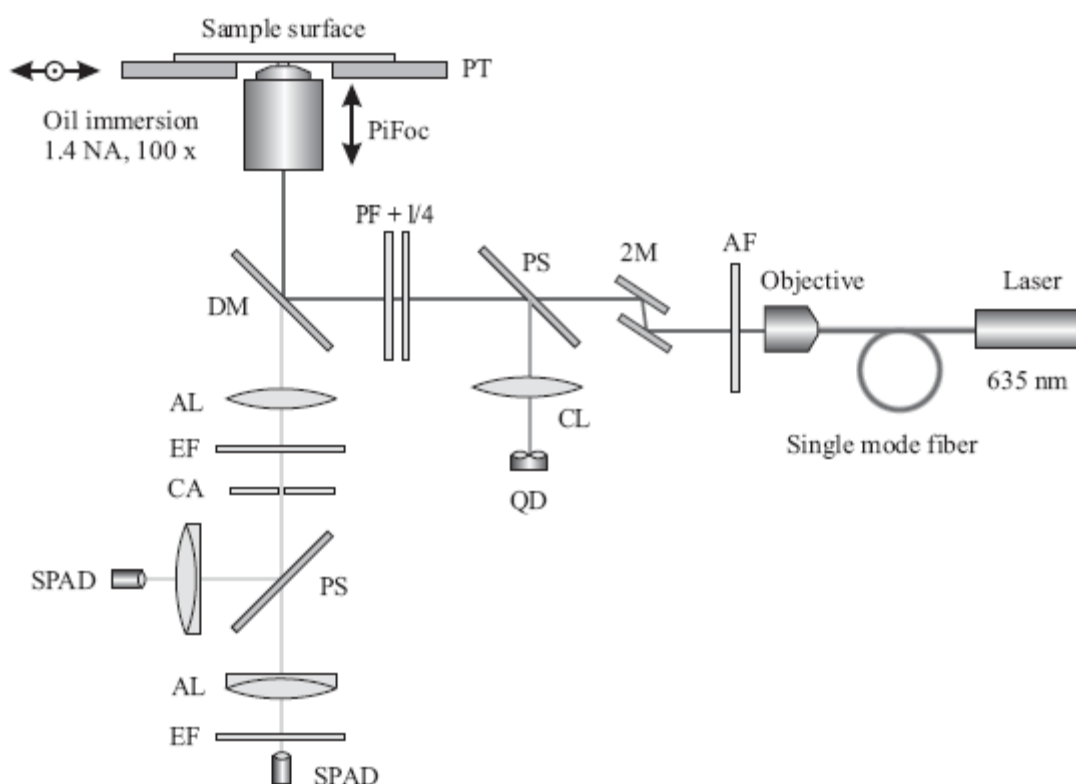
Figure 1.5 An example image showing the schematic of the experimental setup for the laser scanning confocal microscope. (AF: excitation filter, 2M: two-mirror beam steering, PS: polarizing beam splitter, PF+1/4: polarizer and λ/4-plate, DM: Dichroic mirror, EF: emission filter, AL: achromatic lens, CA: Confocal aperture, SPAD: Single photon avalanche diode, PT: Piezo stage, PiFoc: linear piezo actuator, CL: Cylindrical lens, QD: Quadrant diode) [41].

1.7.3 Experimental Components for Excitation and Detection of Fluorescence

In this part, the key experimental components that are needed to setup TIRF microscopy setup are introduced.

1.7.3.1 Light source

Lasers are always of interest for single molecule excitation due to their high spatial mode quality, their intensity and their spectral purity. In our experiments, we use solid state continuous wave green laser (λ=532 nm).

1.7.3.2 Dichroic Mirror

Dichroic mirror is used as a reflector for the specific range of wavelength and as an emitter for other wavelength simultaneously. In fluorescence process, as the emission wavelength is longer than the excitation wavelength due to Stoke's shift, dichroic mirror is used to separate the excitation laser from the fluorescence emission of single molecules before the fluorescence is sent to detector.

1.7.3.3 Microscope Objective

Microscope objective is the key component for every microscope since the power of magnification of small objects is determined by it. It is used not only to apply the excitation laser to the probe but also to collect the emission from the probe molecules.

In principle, a microscope is used to magnify the small objects. The resolution of the image is limited by diffraction and the smallest resolvable distance between two point sources is defined for a given wavelength as in the following equation by the diffraction theory.

$$d_{\min} = 1.22 \frac{\lambda}{2N.A.} \tag{1.2}$$

Here, $N.A.$ is the numerical aperture of the objective lens which is defined as;

$$N.A. = n\sin(\theta) \tag{1.3}$$

where n is the index of refraction in the "object space" and θ is the half of the maximum light collecting angle from the object. As the minimum resolvable distance is getting smaller with increasing $N.A.$, the numerical aperture should be as large as possible.

So, well-corrected images of small objects can be presented by good microscope objectives with high $N.A.$. For instance, immersion oil microscope objectives can collect light up to 90° with $1.4\ N.A.$. It is always advantageous if it is possible to collect light through glass or through oil as the numerical aperture is inversely proportional to the refractive index.

With this information, in our experiments, we used $1.49\ N.A.$ oil immersion microscope objectives for higher efficiency of fluorescence collection.

1.7.3.4 Detectors

As stated in section 1.5.1.1, it is advantageous to use EMCCD detectors for recording the images of fluorescence emission from single dyes. So, we use Hamamatsu ImagEM CCD camera in our experiments.

1.7.3.5 Optical Filters

Choosing appropriate optical filters suppressing the reflected and scattered light which doesn't have the fluorescence origin and transmitting the fluorescence emission is also important. So, we tried to select appropriate filters for our experiments.

Chapter 2

MATERIALS AND EXPERIMENTAL METHODS

The main concern in the observation and analysis of our single molecule experiments is related with the dynamical behavior of single molecules which behave as sensitive reporters inside the host material.

With this information in mind, we introduce the host materials (the block copolymers) and the guest materials (the fluorescent dye molecules) that we use through our experiments in the first part of this chapter. In the second part, detailed explanation about why and how we use these materials is stated and the structures that we supposed to obtain is presented.

2.1 Host-Guest Materials Specific to Our Experiments

In our experiments, we incorporated dye molecules to polymer network and tried to characterize the system. In this system, the important thing that we focused on is obtaining the cylindrical channels inside block copolymer thin films which are parallel to the substrate giving the chance to the single fluorescent molecules to make 1-dimensional diffusion inside them. We were also interested in obtaining the lamellar morphology parallel to substrate for observing 2-dimensional diffusion of fluorescent dyes to be able to make comparison between them.

As organic dyes, we used the hydrophilic rhodamine B (figure) molecules as well as the hydrophobic terrylene molecules. As polymer network, we have chosen to study with Polystyrene (PS) and Poly(methyl methacrylate) (PMMA) for some specific experiments

and we have mostly worked with three different Poly(butadiene)-Poly(ethylene oxide) (PB-PEO) diblock copolymers with different molecular weights. The importance and relevance of them with the study are explained in the following section.

The hydrophobic or hydrophilic interactions between polymer network and the organic dyes are first taken into account to make possible the fluorescent dye molecule diffuse inside the preestimated well-formed regions. For instance, The PB block which shows hydrophobic property forms the cylindrical channels inside the PEO crystalline matrix. When the terrylene dye molecules showing hydrophobic characteristic are incorporated with this PB-PEO diblock copolymer system, they choose diffusing inside hydrophobic PB cylindrical channels rather than locating inside hydrophilic crystalline PEO region due to hydrophobic interactions.

Below, the chemical structures of fluorescent dyes and polymer are shown in figure 2.1 and figure 2.2, respectively.
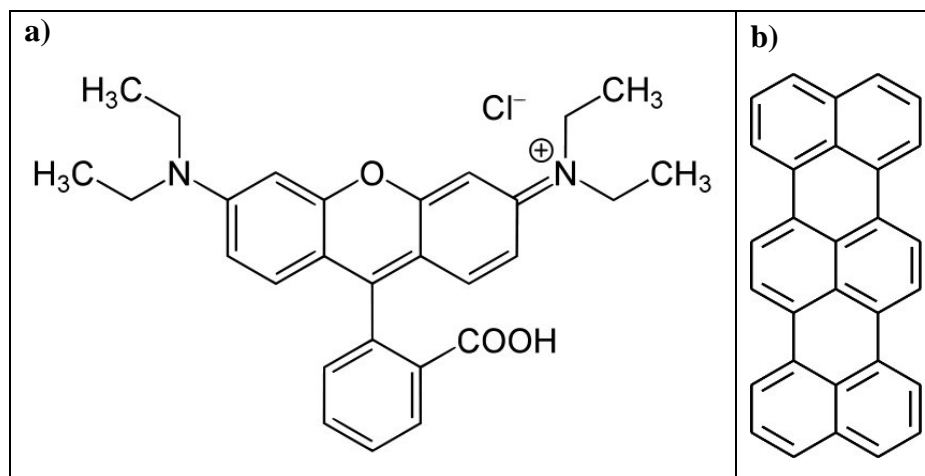
Figure 2.1 Chemical structure of a) hydrophilic rhodamine B and b) hydrophobic terrylene molecules.
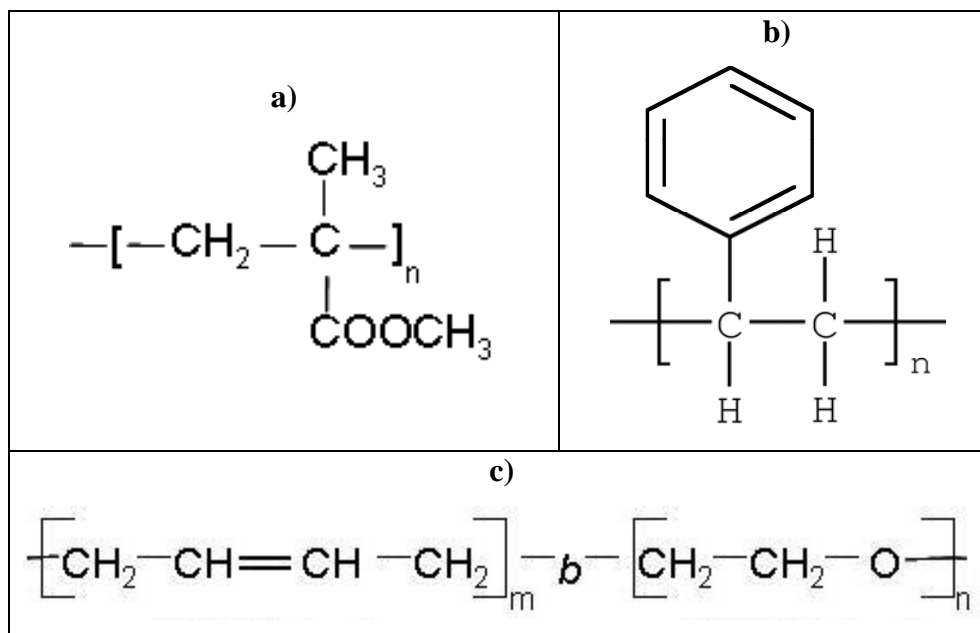
Figure 2.2 Chemical structure of a) PMMA, b) PS and c) PB-PEO diblock copolymer.

2.2 Materials and Methods

We performed single molecule experiments at room temperature. Samples that we used through our experiments were prepared by spin-coating highly diluted dye solution which was mixed with polymer solution at 2000 rpm for 1 minute. After that, dye doped polymer thin films were obtained. In most of our experiments, we needed the thin films to be annealed at specific temperature for specific block copolymer due their characteristic glass transition temperature, T_g and melting temperature, T_m. This was done for several hours so that better channel formation was observed.

2.2.1 Materials

2.2.1.1 Polymers

Before introducing the PB-PEO diblock copolymer and terrylene dyes in detail, it is important to notice that for some specific experiments, PMMA and PS polymers and

rhodamine B dyes were utilized. The reason behind that was the need for a system to image stationary molecules for specific experiments. As PMMA is hydrophilic and amorphous polymer, the hydrophilic rhodamine B molecule was chosen as a guest for incorporation in such experiment. Moreover, PS was sometimes needed as a hydrophobic amorphous polymer for incorporation with the hydrophobic terrylene dye. Working with PB-PEO provided the most important results of our experiments. However, for observation of characteristic single molecule behaviors and calculating the localization accuracy of the experimental setup, these amorphous polymers and hydrophilic dye were needed. In those experiments, highly diluted dye molecules were embedded in very thin films of amorphous polymers.

There are three PB-PEO diblock copolymers which have different molecular weights that were mostly used through this work. Two of them are high molecular weight asymmetric amphiphilic diblock copolymer. They are PB_{593}-PEO_{3705}, PB_{219}-PEO_{1386} (subscripts denote the average number of monomers). In the bulk the hydrophobic and amorphous minor component PB (volume fraction = 0.20) forms cylindrical channels in the matrix of the hydrophilic and crystalline major component PEO. The difference in the morphology between these two polymers is the channel diameter. The diameter of PB_{219}-PEO_{1386} is expected to be smaller than the diameter of PB_{593}-PEO_{3705}. The other polymer is again a high molecular weight polymer but it is symmetric diblock copolymer. It is PB_{593}-PEO_{989} (subscripts denote the average number of monomers) which shows lamellar morphology in the bulk having the volume fraction of PB to be 0.49. PB_{593}-PEO_{3705}, PB_{219}-PEO_{1386} and PB_{593}-PEO_{989} are named as P2327, P1945C and P2325, respectively. They are commercially available products by Polymer Source Inc. Use of P2327 and P1945C gives the opportunity of comparing single molecule diffusion inside the same morphology in narrower and broader 1-dimensional channels. Additionally, use of P2325 makes it possible to monitor the confinement of single molecule diffusion from 2-

dimensions to 1-dimension due to the high amount of decrease in diffusion coefficient from 2-dimensional diffusion to 1-dimensional diffusion. Below, the expected self-assembled morphology of PB-PEO can be seen in figure 2.3.
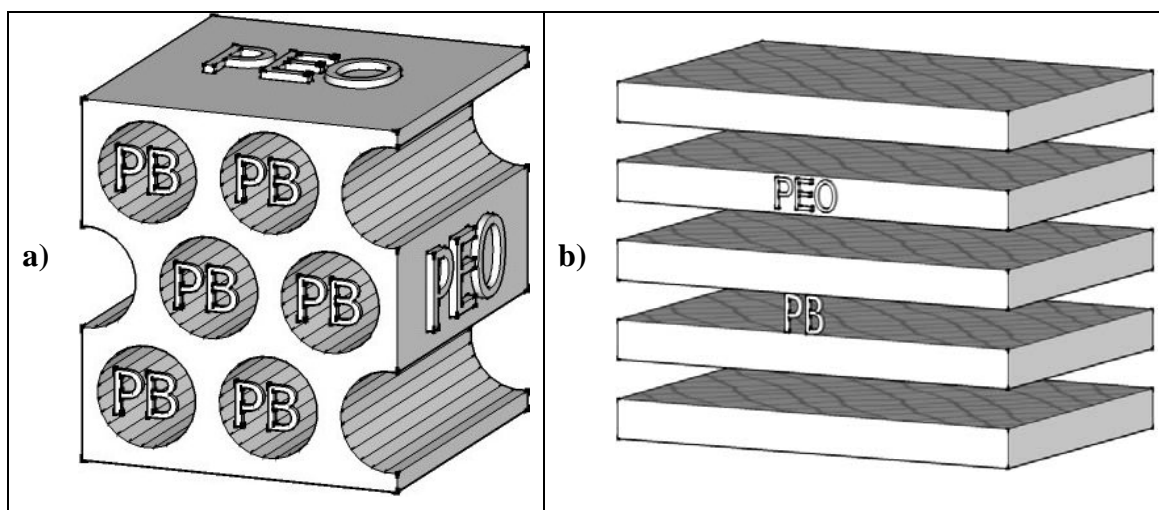
Figure 2.3 Schematic representation of self-assembled morphology in a) P2327 and P1945C and b) P2325 diblock copolymers.

2.2.1.2 Probe Molecules

Although we needed to use rhodamine B molecule as a reporter for some experiments, terrylene molecule was very good candidate as a probe since its photostability is better than most of other dyes [48]. So, it was mostly utilized. It was also suitable for single molecule applications in our experiments such that terrylene is a hydrophobic fluorescent dye and it goes selectively to the amorphous PB block due to hydrophobic interactions after the sample is prepared. This makes it possible to observe the diffusion inside the formed channels of PB in PEO crystalline matrix on the sample surface as we discussed in section 2.2.1.1.

2.2.2 Methods

2.2.2.1 The Preparation of Thin Films

For the preparation of thin films of amorphous homopolymers having highly diluted dye solutions, 0.3 mL 2nM RhodamineB/Chloroform solution is mixed with 2.7mL 3mg/mL PMMA/Chloroform solution and 2mL 20 nM Terrylene/Toluene solution is mixed with 1 mL 40 mg/mL PS/Toluene solution.

For obtaining diblock copolymer thin films with dye molecules, block copolymer solution and dye solution is first prepared. The appropriate concentration of terrylene and diblock copolymer solution is tried to be determined for obtaining the desired morphology inside the desired thickness of the film after numerous trial and error. The concentration of diblock copolymer determines the thickness of the coated sample and it needs to be at sufficient values for the formation of channels. The concentration of terrylene also has to be at an adequate level for single molecule observation. For instance, if the concentration is too high, then the only observation is a big bright spot; if it is too low, may be the things that are observed are some scattered light from dust or other scatterings from the sample. So, for solution preparation of P2327 and P1945C, we mix 1mL 40 mg/mL PB-PEO/Toluene with 3mL 20 nM Terrylene/Toluene solution which results in a solution containing ~10mg/mL PB-PEO/Toluene and 15nM terrylene dye molecules. They are called as thin P2327 film and thin P1945C film throughout this thesis to make it easy for understanding and telling. We also prepared samples from P2327 and P1945C by doubling the concentration of polymer solution which makes 80 mg/mL to double the film thickness on the coverglass. The final solution contains ~20mg/mL PB-PEO/Toluene and 15nM terrylene dye molecules. And they are called as thick P2327 film and thick P1945C film throughout this thesis. For the solution preparation of P2325, we mix 1 mL 20 mg/mL P2325/Toluene solution with 3 mL 20 nM Terrylene/Toluene solution. This solution ends in a solution containing 5mg/mL P2325 and 15 nM terrylene. The aim of using P2325 is

the observation of 2-dimensional diffusion of terrylene molecules. The concentration is kept at small values to let the film preparation with one period of PB-PEO on cover glass allowing the 2-dimensional diffusion. Samples of these solutions were then prepared by spin coating them at 2000 rpm for 1 minute on glass substrates. Finally, there are 5 different samples to make comparison between them which are summarized in the following table.

Sample#1: Thin P2327 Film	Sample#2: Thin P1945C Film
15nM Terrylene doped 10mg/mL P2327	15nM Terrylene doped 10mg/mL P1945C
Sample#3: Thick P2327 Film	Sample#4: Thick P1945C Film
15nM Terrylene doped 20 mg/mL P2327	15nM Terrylene doped 20 mg/mL P1945C
Sample#5: P2325 Film	
15nM Terrylene doped 5 mg/mL P2325	

Table 1 List of the prepared samples.

The resulting P2327, P1945C and P2325 films are then annealed at 65°C, 58°C and 70°C for better channel formation, respectively. The thickness of thin P2327 film was (measured with Ellipsometry to be) between 50-60 nm. This shows that well formed cylindrical PB channels parallel to the substrate inside the PEO crystalline matrix could be well formed for thin and thick P2327 and P1945C films. The illustration of the self-assembled morphology for thin P2327 and P1945C films is shown in figure 2.4. For thick P2327 and P1945C films, a second layer of full PB channel or more is expected to be formed.
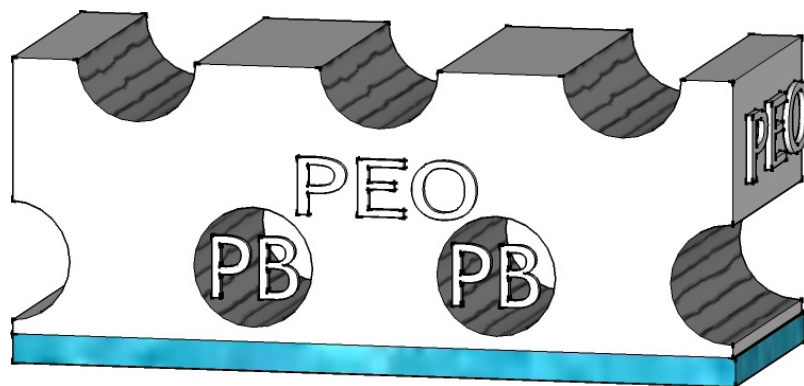
Figure 2.4 The illustration of the expected self-assembled morphology on cover glass.

2.3 Determination of Surface Topography with Atomic Force Microscopy and Scanning Electron Microscopy

The prepared samples of P2327 and P1945C were analyzed with AFM and SEM for the observation of surface morphology. After obtaining the trajectories of single molecules inside the cylindrical channels of PB-PEO, the AFM and SEM images were tried to be correlated with the trajectories. Below, a typical AFM image of PB-PEO film surface is shown in figure 2.5.
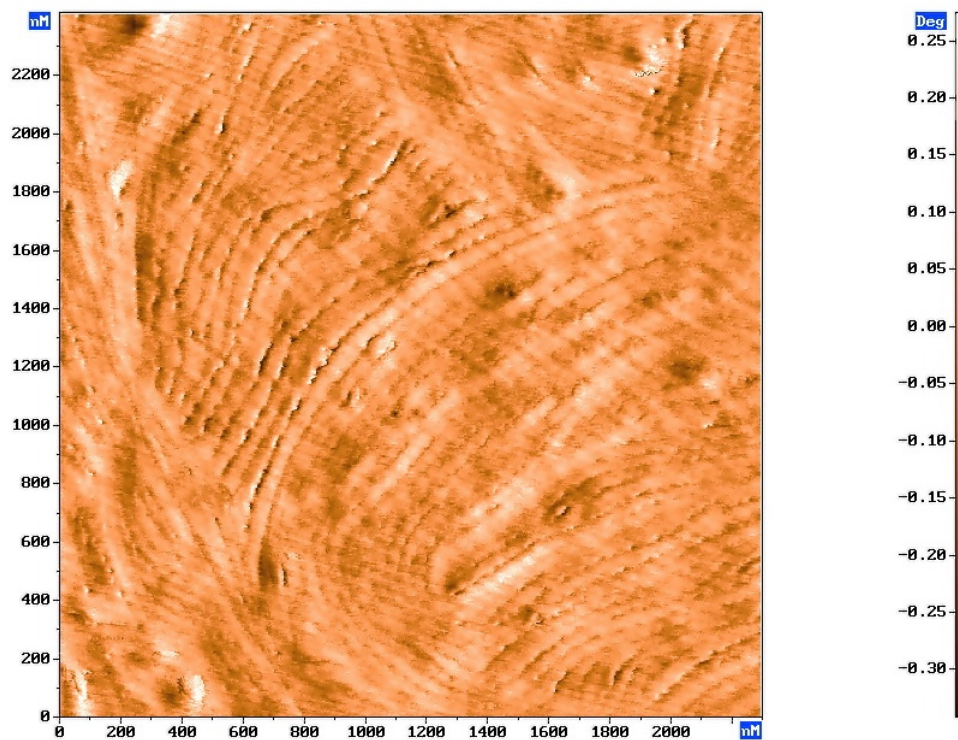
Figure 2.5 AFM image of PB-PEO thin film surface.

In figure 2.5, the dark regions correspond to PB channels where the bright regions correspond to PEO crystal barriers.

Chapter 3

SINGLE MOLECULE TECHNIQUES

3.1 Introduction

There are important things to consider about for and after the observation of single molecules. In this chapter, first, the total internal reflection fluorescence microscopy setup that we used for detecting fluorescent dyes is described and shown. When some images are collected using this setup, they are just bright spots without deciding whether they are real single molecules or not. So, to be sure that they are real single molecules, we show some of the results from our single molecule observation dealing with the characteristics of them. Then, the thing left behind is having their trajectories inside the host structure and dealing with them. So, we first show the localization accuracy of our experimental setup in positioning single dye molecules. After that, we describe, how and what we do with single molecules in detail in this chapter.

3.2 Single Molecule Observation by TIRF Microscopy

The experiments for the observation of single molecule were performed at room temperature (~25°C) which was above the glass transition temperature of the PB block (~-10°C) and below the melting temperature of the PEO block (~58°C-65°C). This allowed the movement of the probe molecules in PB channels while the crystalline PEO block provided the confinement barriers.

For the observation of single molecule, we performed our experiments by using objective type TIRF microscopy. In our experimental setup, a continuous wave green laser

(λ=532 nm) was used for excitation in the inverted geometry. It was first expanded by a telescope and then reflected by a mirror and focused by another lens to the back of the microscope. This laser beam was further reflected by a dichroic mirror and sent to the back aperture of a high numerical aperture microscope objective (N.A. = 1.49, 60x, oil immersion) for wide field illumination. Doing this, the sample and so the fluorescent dyes were excited by the laser light passing through the objective according to the epi-fluorescence microscopy principles [46]. After obtaining wide-field illumination, the angle of incidence of the laser beam to the polymer/air interface was further adjusted so that the total internal internal reflection of the laser beam was observed to minimize the background noise as we described in section 1.5.1. The fluorescence emission coming from the fluorescent dyes (rhodamine B or terrylene) was collected by the same microscope objective and separated from the excitation laser by the use of a dichroic mirror. Then, it was sent through 1.5x magnification element inside the microscope, a 2x further magnification and a bandpass filter. TIRF microscopy images were then recorded with an Electron Multiplied Charged Coupled Device camera (Hamamatsu-ImagEM). The exposure time for recording the fluorescence images was 0.1 second which corresponds to 10 frame/sec for movies discussed in this study.

Below, the schematic and the photograph of the experimental setup are shown in figure 3.1 and 3.2, respectively.
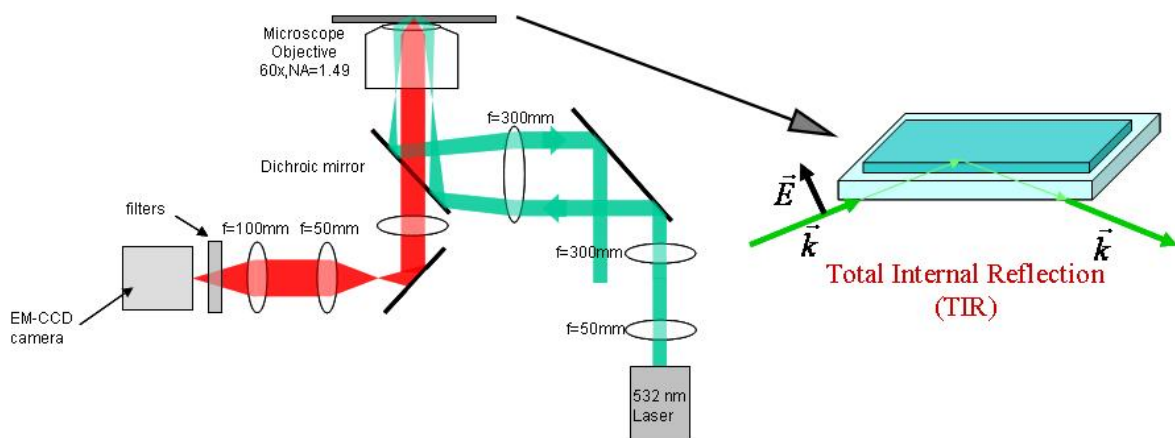
Figure 3.1 The schematic of TIRF microscopy setup used in the experiments.
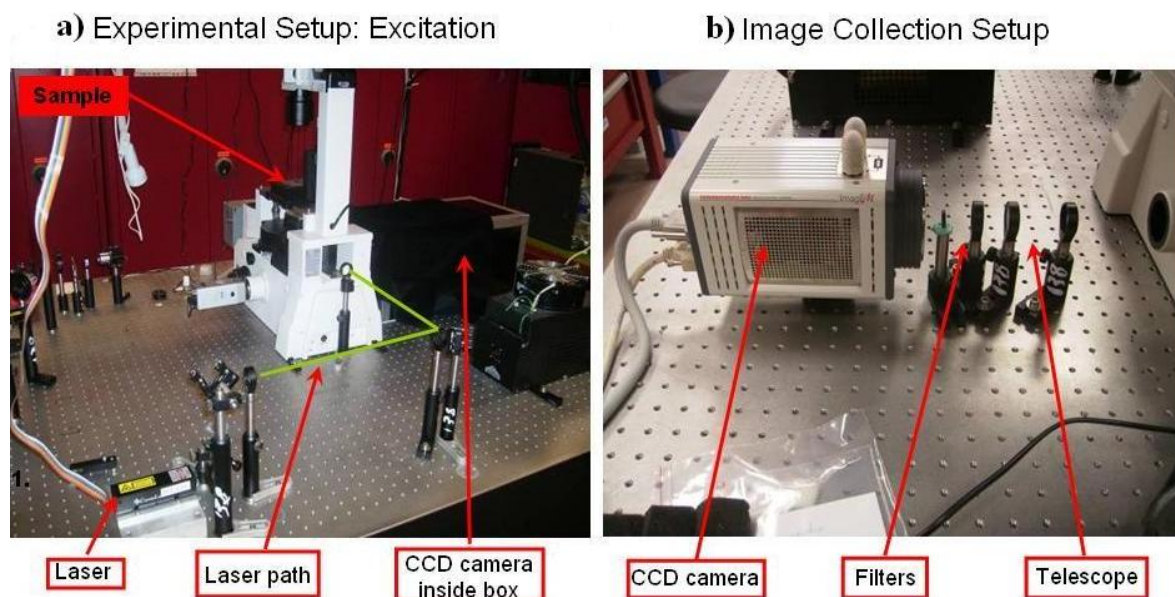
Figure 3.2 The photographs of the a) excitation and b) image collection setups.

3.3 Characteristic Behavior of Single Molecules

The blinking which shows consecutive on-and-off behavior in the intensity of single rhodamine B molecule and the photobleachings of single rhodamine B and terrylene molecules which end their fluorescence at one single step disappearing from the

observation are shown in the following figures (Figure 3.3, 3.4 and 3.5) as an indication of their being real single dye molecules.
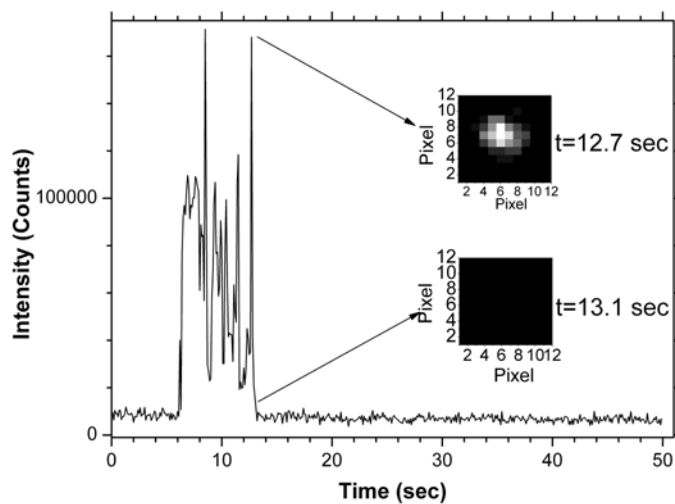
Figure 3.3 Blinking of single rhodamine B molecule in PMMA thin film.
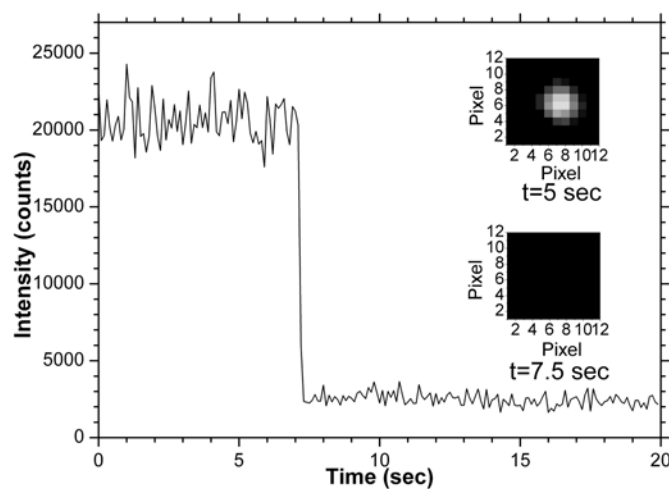
Figure 3.4 Photobleaching of rhodamine B molecule inside PMMA thin film. Insets show the image of the molecule before and after photobleaching.
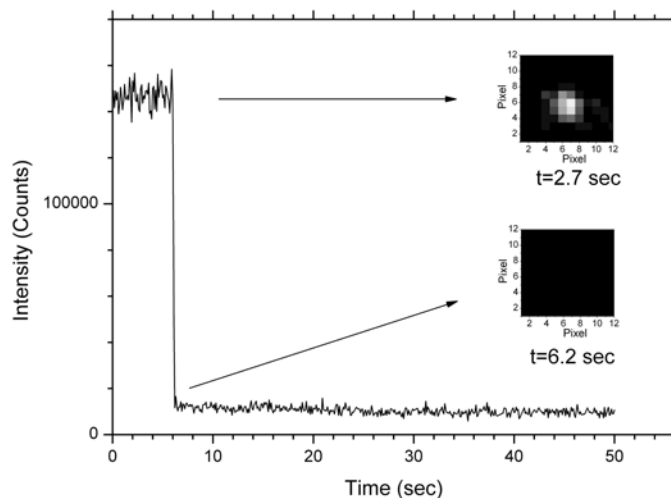
Figure 3.5 Photobleaching of single terrylene molecule. Insets show the image of the molecule before and after photobleaching.

3.4 Localization Accuracy of Single Molecules in Thin Films

Recent developments in imaging of single fluorescent dye molecules make it possible to explore the nanostructured channel systems with very high resolution. By recording the fluorescence images of dye molecules at high signal to noise ratios, it was possible to achieve spatial resolutions of several nanometers. In the work of Yildiz *et.al*, they were able to show that they can resolve the displacement of a single molecule with a displacement of as small as ~1.5nm by using a standard TIRF microscopy [4]. This technique is named as fluorescence imaging with one nanometer accuracy (FIONA) by them.

The basic idea of FIONA is based on accurately determining the center of the image which corresponds to the position of the dye molecule. With the position information of the dye molecule before and after a step, the minimum resolvable displacement is determined. This is done by fitting the X-Y profile of the image to a Gaussian function [4]. Then, mean

value of the distribution, $\mu = (x_0, y_0)$ and the standard error of the mean σ_μ is determined. Here, σ_μ corresponds to the standard positioning error which is given as in the following equation:

$$\sigma_{\mu_i} = \sqrt{\left(\frac{s_i^2}{N} + \frac{a^2/12}{N} + \frac{8\pi s_i^4 b^2}{a^2 N^2} \right)} \qquad (3.1)$$

where N, a, b and s_i correspond to the number of collected photons, the pixel size of imaging detector, the standard deviation of the background, the width of the distribution (standard deviation in the direction, i), respectively.

By using the information that we described above, we performed the calibration experiments by imaging the stationary single rhodamine B dye molecules inside PMMA polymer host and terrylene dye molecules inside PS polymer host. The samples containing rhodamine B and terrylene molecules were translated with 20nm and 30 nm step size using a piezoelectric stage, respectively. Then, the step sizes of the translation stage for the samples containing rhodamine B and terrylene molecules were measured as 21.83nm with 1.48nm standard deviation (Figure 3.6) and 30.23 nm with standard deviation of 1.48 nm (Figure 3.7), respectively. Here standard deviations show the resolution of our experimental setup in positioning the single rhodamine B and terrylene dye molecules, i.e. positioning error. So, the resolution of our experimental setup in positioning single dye molecules is ~1.5 nm.
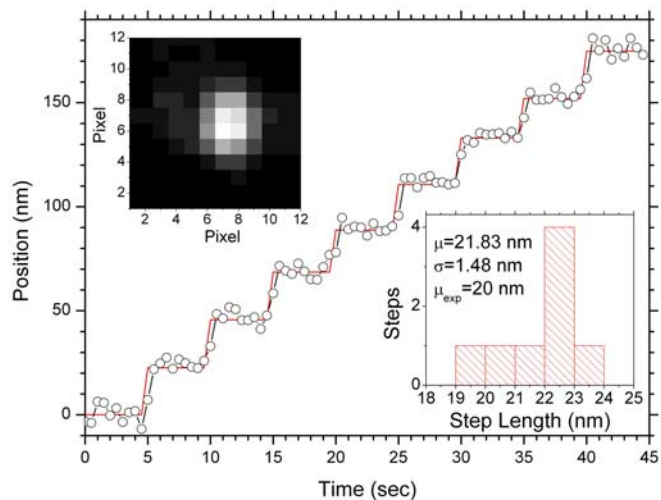
Figure 3.6 Result of the calibration experiment of localizing single rhodamine B molecule. 20 nm step size of piezoelectric stage was measured as 21.83 nm with a positioning accuracy of 1.48nm.
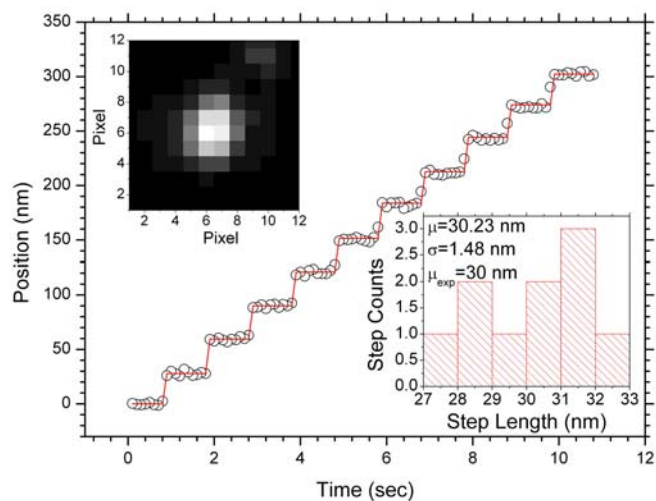
Figure 3.7 Result of the calibration experiment of localizing single terrylene molecule in PS. The 30 nm step size was measured to be 30.23nm with a positioning accuracy of 1.48 nm.

Moreover, to determine the typical signal to noise ratios and localization accuracies in our experiments, single molecule trajectories were first determined by using the particle tracker plugin that is described in the following sections (Section 3.6). At each frame, a two dimensional Gaussian fit was performed in a 12x12 pixel^2 area centered at the coordinates found by the particle tracker software. Localization accuracies were then calculated using the expression [49, 32];

$$\sigma(r) = \sqrt{3.53 \left[\sum_{i=-N_x}^{N_x} \sum_{i=-N_y}^{N_y} \frac{\left(I_0^2 x_i^2 / \sigma_{xy}^4 \right) \exp\left[-\left(x_i^2 + y_i^2 \right) / \left(2\sigma_{xy}^2 \right) \right]}{\sigma_{bg}^2 + \sigma^2 \left(I(x_i, y_i) \right)} \right]} \qquad (3.2)$$

where I_0, N_x, N_y, x_i, y_i, σ_{xy}, σ_{bg}^2, and $\sigma^2\left(I(x_i, y_i)\right)$ correspond to the maximum intensity, number of pixels in the x and y directions, x and y coordinates, the standard deviation of the Gaussian, variance of the background intensity, and the local variance of the signal intensity at the position (x_i, y_i), respectively. Our experimental conditions revealed typical signal to noise ratios and localization accuracies of around 4 and 8 nm, respectively.

3.5 Translational Diffusion

The probable movement of small particles in a solution is called as Brownian motion. Calculation of the means square displacement (MSD) as a function of lag time, τ, for the movement of small particles is used for characterizing the movement by diffusion coefficient which is a measure of the speed of diffusion [46].

Brownian motion can be observed in different environments having dynamical property in different nature, i.e. rotational, translational etc. In our system, we concentrate on translational displacement, in other word, the random walk, of single dye molecule inside 1- and 2- dimensional regions in polymer thin films. In random walk, the MSD of a diffusing particle in n dimensions is given as in the following equation:

$$\left\langle \left| \vec{r}\left(t+\tau\right) - \vec{r}\left(t\right) \right|^{2} \right\rangle = MSD\left(\tau\right) = nD\tau \qquad (3.3)$$

In the following sections, it is described how to calculate MSD for corresponding τ. Moreover, different mathematical formulas describing the time dependence of the MSD for some different specific cases are given and explained briefly.

3.6 Automated Program for Getting the Trajectory of Diffusing Single Molecules

A huge amount of raw data is obtained after finishing the experiment using the setup described in section 3.2. It is firstly in the form of a recording showing the diffusion of individual particles. Each sequence of the recording has the intensity information as well as the position information of individual dye molecules. In the evaluation of this data the particle tracker plugin [50] implemented for the program called ImageJ [51] was used. The algorithm of this plugin which is described in [52] first detects the single molecules in every frame of the recording and then it links the position information to form the trajectory of the molecule. In the following, the interface of the ImageJ program and particle tracker plugin is shown (Figure 3.8).
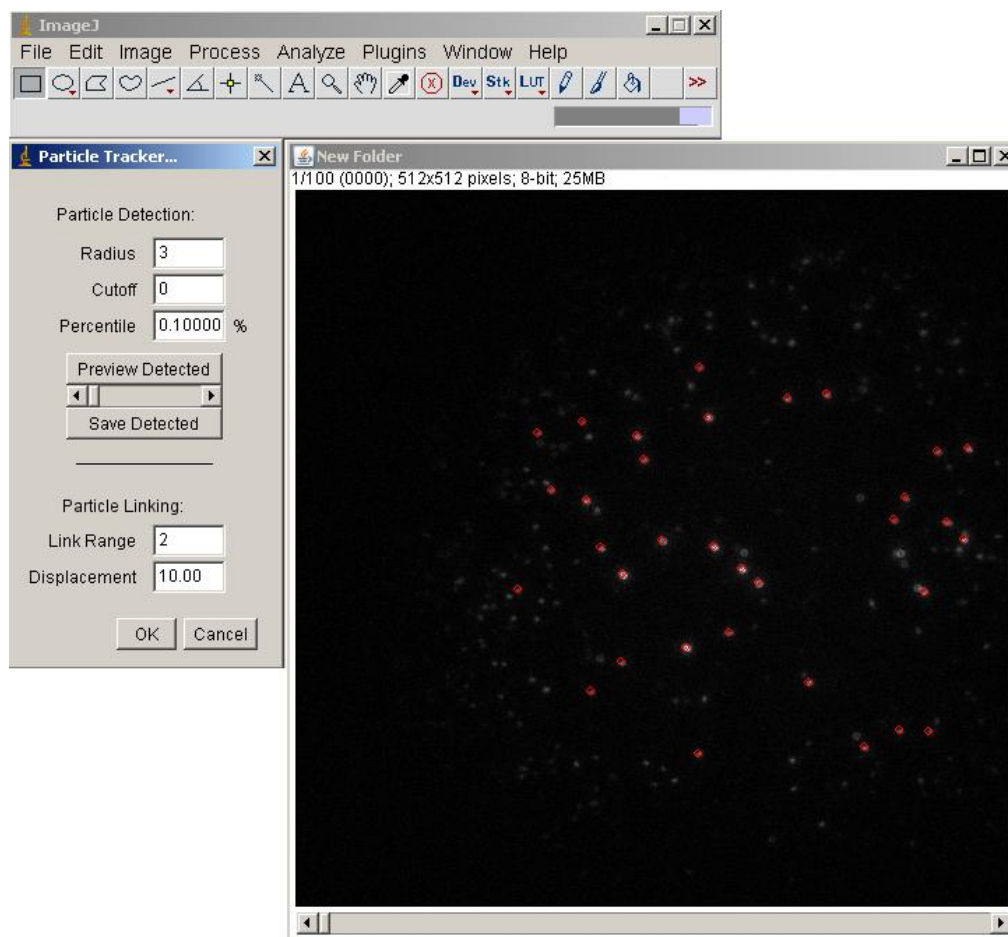
Figure 3.8 Interface f of ImageJ program and Particle Tracker Plugin of ImageJ.

This plugin of ImageJ is very advantageous as a tracking tool since it is very easy to use and computationally efficient. By this way, it is very-well suited for analyzing videos of low-intensity fluorescence microscopy. As an input, frame by frame separated images or ASCII files of a video or a video itself can be used. The algorithm first estimates the locations of single molecules through the local intensity maxima information of single molecules and then refines these position information by making 2D Gaussian fits to the selected bright structures. Finally, it links the position information to create the trajectories.

As an output, all found trajectories and the original movie frames in an overlay can be visualized (Figure 3.9).
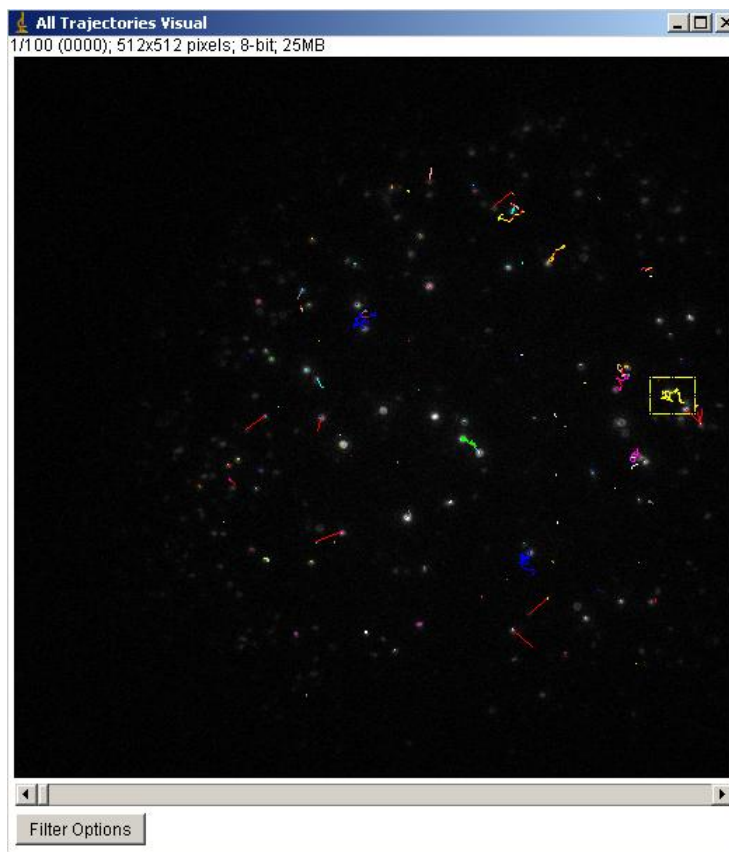
Figure 3.9 Visualization of the obtained trajectories using Particle Tracker Plugin.

Furthermore, the position information of single molecule in every trajectory can be saved in a single .txt file for further analyzing. It is also possible to visualize each trajectory separately and the position information of the selected trajectory can be saved individually (Figure 3.10).
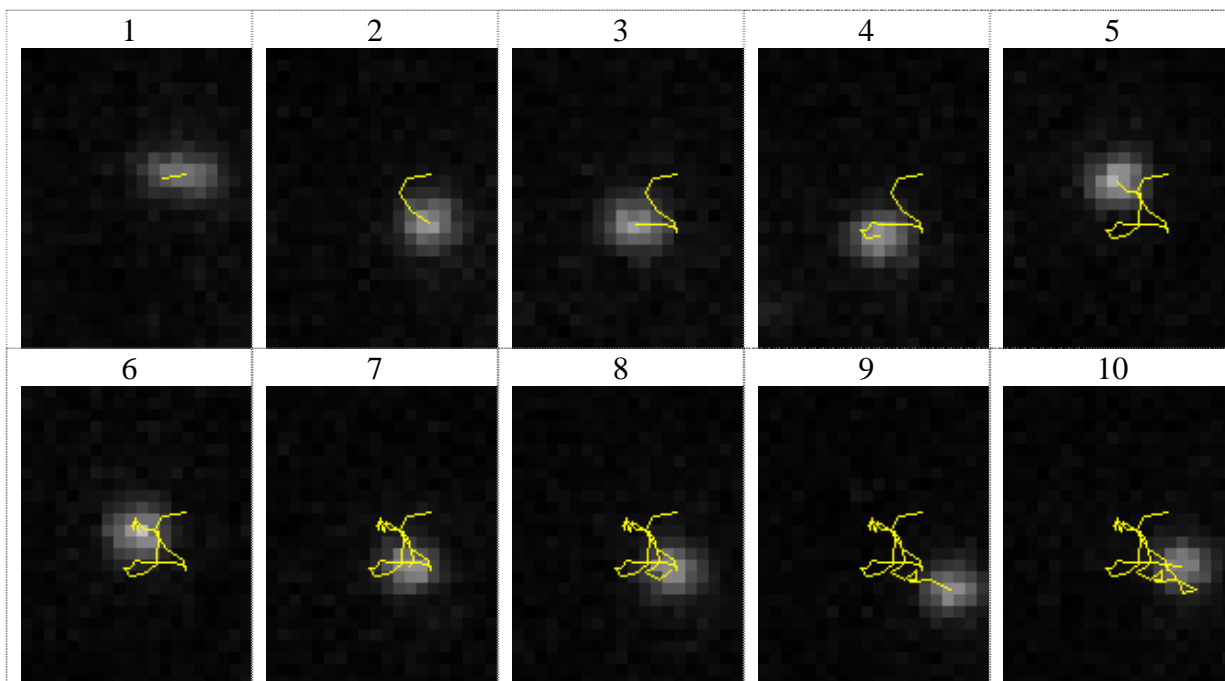
Figure 3.10 The trajectories after consecutive 5 frame of a diffusing single molecule obtained from a video recorded with a frame rate of 15 frame/sec.

The individual visualization of the trajectory of single molecules can also be saved in .gif format for later observation without the necessity of running the whole program from the initial step.

3.7 Home Built Program for the Detection of Trajectory

A LabVIEW program which makes 2D Gaussian fits to the patterns originating from the fluorescence of single molecule is prepared for the use in calibration experiments of positioning single dye molecules. This program is fed by the results of ImageJ to find the position of single molecule in the 512x512 pixel^2 recorded images. The molecule is chosen in a 12x12 pixel^2 area since the diffraction limited area is 4x4 pixel^2 in the 180x magnified recorded images. The fluorescence intensity in this area is compared with the following equation and the constants are then computed according to this fit;

$$I(x, y) = b + A \cdot \exp\left(-\frac{(x - x_m)^2}{2\sigma_x^2} - \frac{(y - y_m)^2}{4\sigma_y^2} \right) \tag{3.4}$$

and the measured constants allows to the calculation of signal to noise ratio with the following equation:

$$SNR = \frac{A}{\sqrt{A + b}} \tag{3.5}$$

The interface of the program is shown in figure 3.11 and 3.12. We could obtain the SNR of ~200 and reach the positioning accuracy of single molecule of ~1.5 nm with our TIRF microscopy setup.
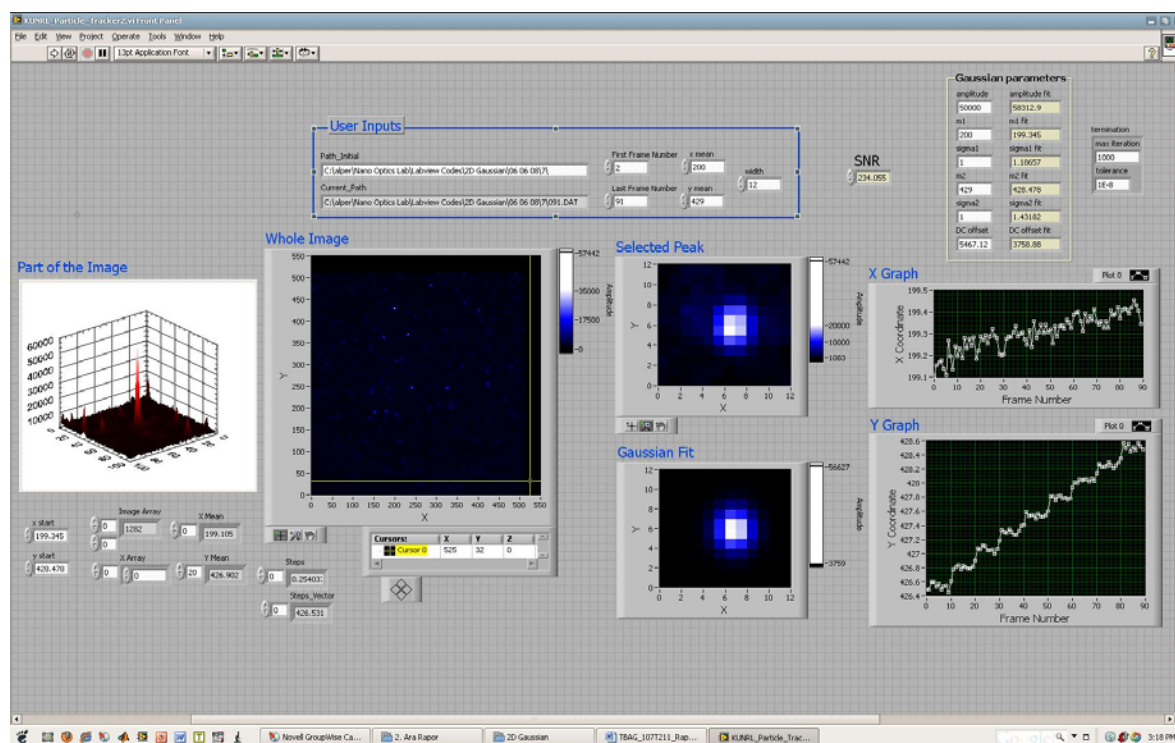
Figure 3.11 Interface (front panel) of the LabVIEW program prepared for calibration experiments.
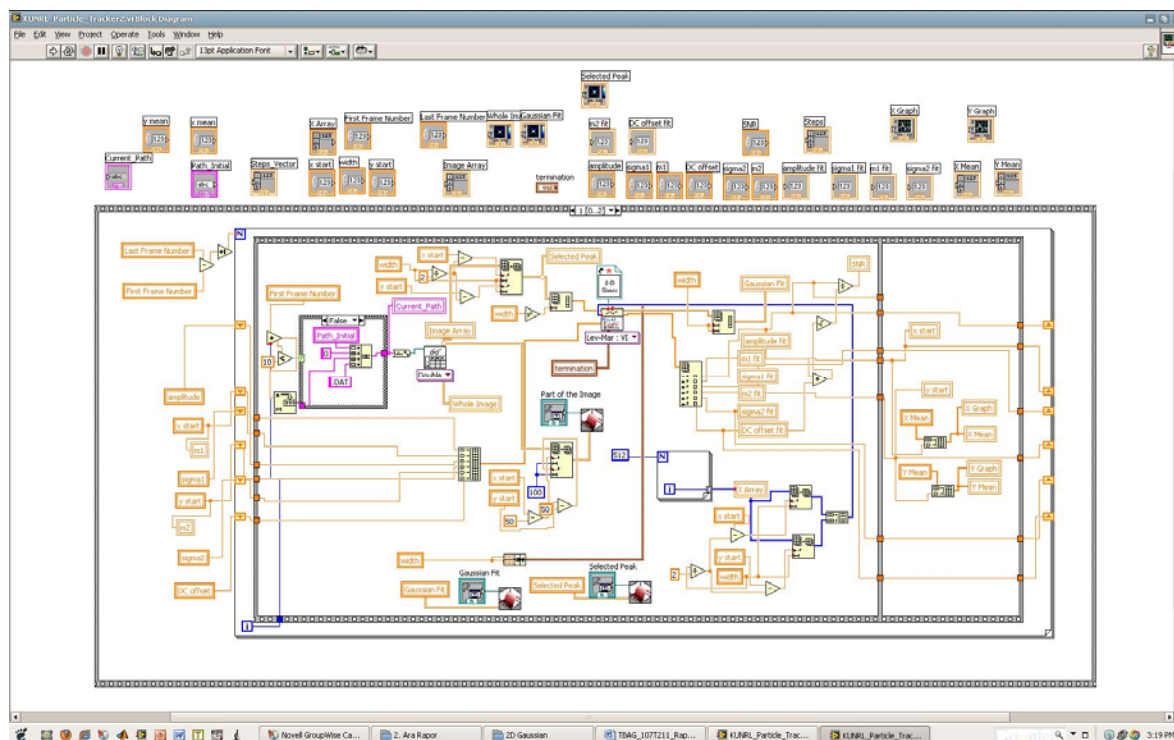
Figure 3.12 Block diagram of the prepared LabVIEW program.

3.8 Mean Square Displacement Calculation

After obtaining the trajectory of a single molecule, calculating the mean square displacement for every lag time (τ) and plotting it as a function of corresponding τ is essential to characterize its mode of motion. *MSD* is determined by using the position information $(r_1(x_1, y_1), r_2(x_2, y_2), r_3(x_3, y_3), \cdots)$ of single molecules in the recorded trajectory at a fixed acquisition time, δt. Lag time is given as $\tau_n = n\delta t$ where n is the number of lags taken between every two steps for the calculation of *MSD* in the trajectory of the molecule.

For instance, for $\tau_1 = 1\delta t$, the displacements are calculated as follows;

$$x_1 = x(t_1) \qquad x_2 = (t_1 + \tau_1) \qquad \Delta x_1(\tau_1) = x_2 - x_1$$
$$y_1 = y(t_1) \qquad y_2 = (t_1 + \tau_1) \qquad \Delta y_1(\tau_1) = y_2 - y_1$$
$$\vdots \qquad\qquad\qquad\qquad\qquad\qquad\qquad\qquad\qquad (3.6)$$
$$x_i = x(t_i) \qquad x_2 = (t_i + \tau_1) \qquad \Delta x_i(\tau_1) = x_{i+1} - x_i$$
$$y_i = y(t_i) \qquad y_2 = (t_i + \tau_1) \qquad \Delta y_i(\tau_1) = y_{i+1} - y_i$$

Then the square displacements are calculated as ;

$$(\Delta r_1(\tau_1))^2 = (\Delta x_1(\tau_1))^2 + (\Delta y_1(\tau_1))^2$$
$$(\Delta r_2(\tau_1))^2 = (\Delta x_2(\tau_1))^2 + (\Delta y_2(\tau_1))^2$$
$$\vdots \qquad\qquad\qquad\qquad\qquad\qquad\qquad\qquad (3.7)$$
$$(\Delta r_i(\tau_1))^2 = (\Delta x_i(\tau_1))^2 + (\Delta y_i(\tau_1))^2$$

The *MSD* is obtained as an average of all steps corresponding to a single lag time by dividing the sum of square displacements to the number of sample periods between start and end points in the trajectory.

$$MSD(\tau_1) = \langle \Delta r(\tau_1)^2 \rangle = \frac{1}{n}\left((\Delta r_1(\tau_1))^2 + (\Delta r_2(\tau_1))^2 + (\Delta r_2(\tau_1))^2 + \cdots\right) = \frac{1}{n}\sum_{i=1}^{n} r_i^2(\tau_1) \quad (3.8)$$

To make it easy for understanding, the calculation is illustrated in the following simple trajectory.

Assume that the following is the trajectory of the molecule for a fixed acquisition time;

For $\tau_1 = 1\delta t$ the *MSD* is calculated for the following lags;
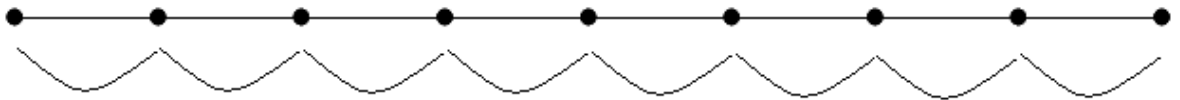
For $\tau_2 = 2\delta t$ it is calculated for the following lags;
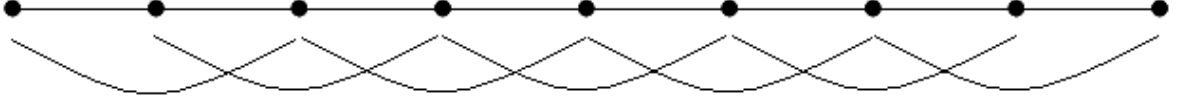
With n lags in the trajectory, the number of individual lags leading to a mean square displacement at a lag time $\tau_1 = 1\delta t$ is n; the number of lags leading to a MSD at a $\tau_2 = 2\delta t$ is $n-1$, for $\tau_3 = 3\delta t$, it is $n-2$, etc. With this information in mind, for instance, when we perform square displacement calculation for $\tau_2 = 2\delta t$, we obtain them as in the following;

$$
\begin{array}{lll}
x_1 = x(t_1) & x_3 = (t_1 + \tau_2) & \Delta x_1(\tau_2) = x_3 - x_1 \\
y_1 = y(t_1) & y_3 = (t_1 + \tau_2) & \Delta y_1(\tau_2) = y_3 - y_1 \\
\vdots & & \\
x_i = x(t_i) & x_3 = (t_i + \tau_2) & \Delta x_i(\tau_2) = x_{i+2} - x_i \\
y_i = y(t_i) & y_3 = (t_i + \tau_2) & \Delta y_i(\tau_2) = y_{i+2} - y_i
\end{array}
\tag{3.9}
$$

And this calculation is done for every lag time, τ_n. By this way, the MSD is calculated for every lag time $\tau_n = n\delta t$ and plotted against it. As a consequence, the statistical error for the MSD increases with the observation time. By this way, we generally use the half of MSD for determination of different motion modes of an individual dye molecule [46].

The important advantage of this calculation is based on the observation of different characteristic curves. So, it provides the ability of resolving modes of motion of individual molecules. Several modes of motion can be observed such as Diffusion with drift, normal diffusion, anomalous diffusion and corralled motion which are described in the following section in detail.

3.8.1 Different Modes of Motion

Various modes of motion can be observed and each of these modes can be identified by plotting the MSD against τ as seen in the following figure for and individual trajectory of a molecule.
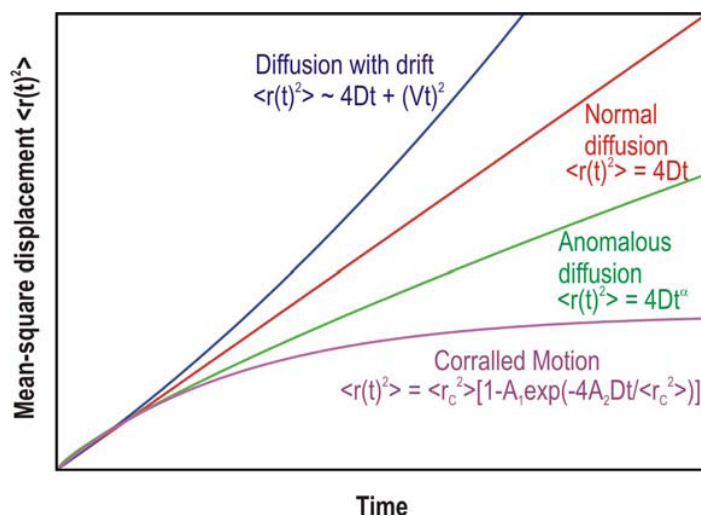
Figure 3.13 Mean square displacement as a function of lag time for 2-dimensional diffusion for different modes of motion including normal diffusion, diffusion with flow (diffusion with drift), anomalous diffusion and confined diffusion (corralled motion) [42].

The above figure is very useful for characterization of the molecule to determine which mode it is belonging to. The following equations show the expected dependence of MSD for the most important modes of molecular motion [42]:

$$\text{Normal diffusion: } MSD(\tau) = 4D\tau \tag{3.10}$$

$$\text{Anomalous diffusion: } MSD(\tau) = 4D\tau^{\alpha}, 0 < \alpha < 1 \tag{3.11}$$

$$\text{Diffusion with flow: } MSD(\tau) = 4D\tau + (V\tau)^2 \tag{3.12}$$

$$\text{Corralled motion : } MSD(\tau) \simeq \left\langle r_C^2 \right\rangle \left[1 - A_1 \exp\left({-4A_2 D\tau} \middle/ {\left\langle r_C^2 \right\rangle} \right) \right], \; A_1, A_2 > 0 \tag{3.13}$$

For an ideal random walk of a single molecule, *MSD* is expected to be in a linear dependence with lag time. When there are some obstacles in the area of its presence, the diffusion is expected to be hindered and the mode of molecule is named as anomalous diffusion. When the area of the molecule prohibits the molecule's motion, it is trapped in an area and it is corralled having a corralled motion. In the presence of effects which provide the flow of molecule, the directed motion of molecule is observed.

In most of our case, directed transport and normal diffusion of the molecules are observed which are discussed in chapter 4.

3.9 Angle Analysis

Calculating the angles between successive steps in the molecule's trajectory is also possible and this also gives further information and sometimes proof about the observed morphology. In order to do this, every angles between two lines which connects the latter and former points of a point to itself (Figure 3.14) are calculated for every point of a trajectory. For single molecule diffusion along a straight line, the histogram of angles should peak around 0 and π radian.
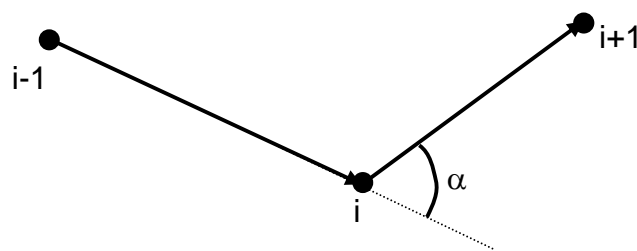
Figure 3.14 Angle between two consecutive steps in a trajectory.

Chapter 4

DIFFUSION OF TERRYLENE DYE MOLECULES IN CHANNELS OF PB-PEO DIBLOCK COPOLYMER THIN FILMS

4.1 Introduction

Diffusion of single terrylene dye molecules in different PB-PEO diblock copolymer thin films was characterized using single molecule microscopy. The main concern was put on the single molecule data which was collected by TIRF microscopy from three different samples of PB-PEO. Motion of single terrylene molecules in 1-dimensional channels of different molecular weight PB-PEO samples and the 2-dimensional Brownian motion of again single terrylene molecules inside another PB-PEO sample were shown. Before doing that, the AFM and SEM images of the obtained samples were first presented in each section to create an insight for the reader about the expected diffusion of molecules. The obtained trajectories of diffusing single molecules were well-correlated to the AFM and SEM results. By this way, the power of single molecule techniques in understanding the morphology and ability of making comparison between these three different polymer systems was demonstrated.

Moreover, the techniques such as calculation of $MSD(\tau)$ as a function of τ and investigation of angles between successive steps were utilized. For instance, angle histograms could prove the presence of single molecule inside the channel, if the cylindrical channel was well-formed and allowed the molecule to make a homogeneous 1-dimensional diffusion. With this information in mind, it was also possible to understand the

inhomogeneities on the samples if present through the observation of single molecule
trajectories or the analyses performed using these trajectories. It is also possible to identify
the mode of motions of single terrylene molecules by using the characteristic curves of
$MSD(\tau)$ as a function of τ. Finally, the diffusion coefficient histograms of terrylene
molecules were well-compared inside different systems and there were significant
differences in single molecule experiment results between these different systems at higher
diffusion coefficients for some specific samples.

4.2 Single Molecule Measurements and Overview of the Trajectories

The fluorescing terrylene dye molecule was excited and the fluorescence emission was
collected as described in section 3.2 for measurements of single molecules. Movies of
about 500 frames were recorded from all samples to follow the diffusion of terrylene dyes
in all 5 different PB-PEO polymer thin films. All movies were recorded at 0.1 second
exposure time and the trajectories were obtained using the particle tracker plugin [50, 52].
The results obtained from the different types of PB-PEO samples are discussed in this
section.

4.2.1 Overview of the Trajectories

In this section, one frame of a recording in which terrylene molecules are diffusing is
shown in figure 4.1a. In figure 4.1b, the typical initial result that is obtained after analyzing
the videos is shown in which the trajectories of diffusing single molecules with the real
image of them were seen in the interface of ImageJ.
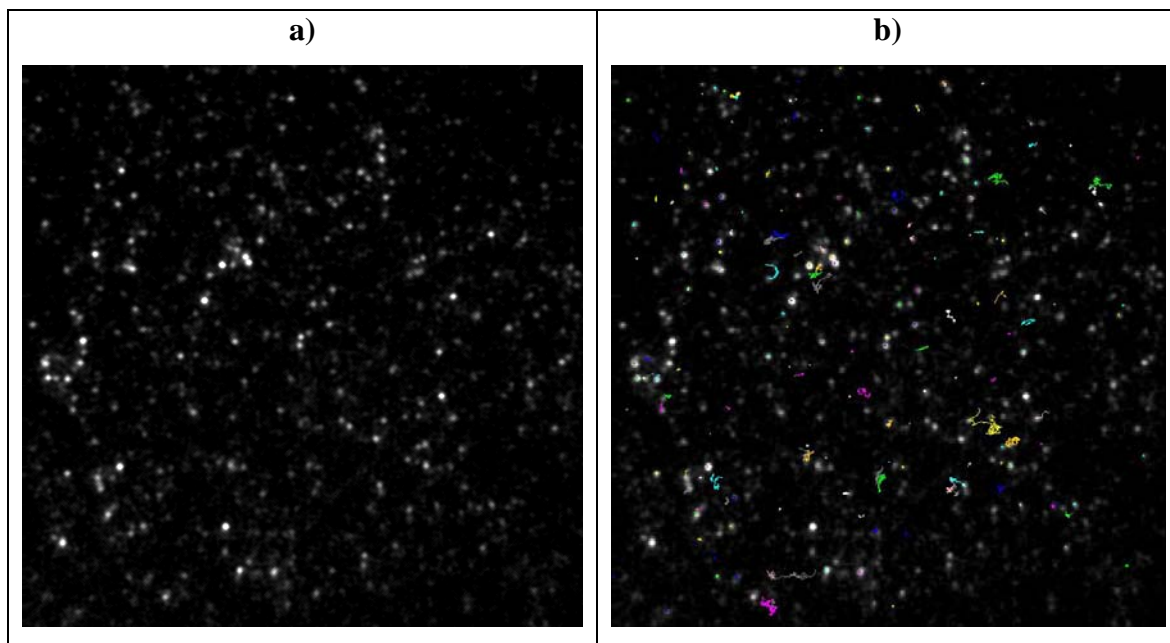
**Figure 4.1 Initial results a) obtained after finishing image collection experiment showing the terrylene
molecules and b) obtained after making first analysis showing the trajectories of diffusing terrylene
molecules.**

All the trajectory information can be accessed as an output. For instance, the trajectories
that were shown in figure 4.1b can be plotted as in the following figure (Figure 4.2).
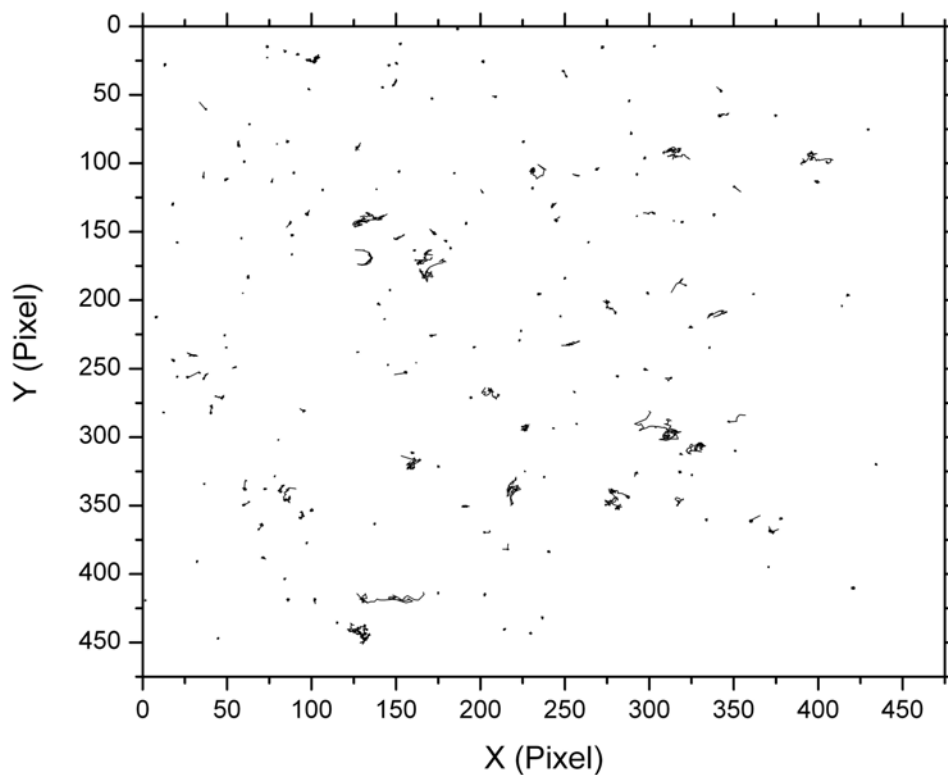
Figure 4.2 Trajectories of single terrylene molecules

There are various modes of motion of diffusing terrylene molecules (Chapter 3.8.1). To make a general overview about the modes of their motion, the $MSD(\tau)$ of every diffusing particle is plotted as a function of τ as seen in figure 4.3.
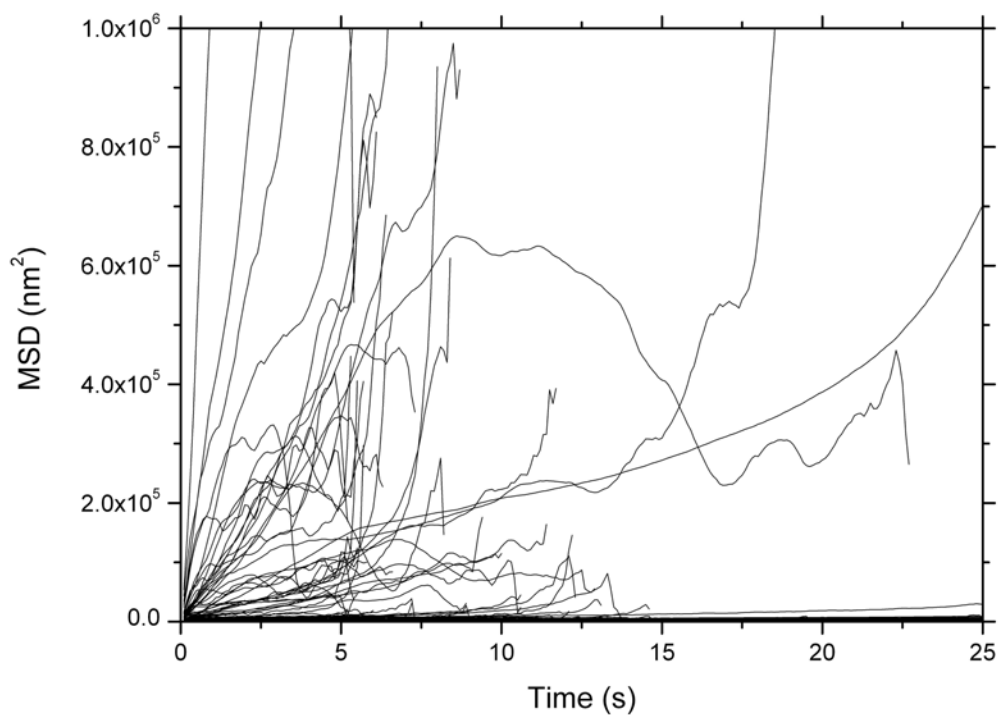
Figure 4.3 The MSD vs. τ of every diffusing single terrylene molecule.

In figure 4.3, the presence of different modes of motion is clear since the parabolic dependence of $MSD(\tau)$ on τ is observed as well as the linear relationship between these two. Furthermore, when we plot the semilog graph of $MSD(\tau)$ vs. τ, it is observable that there is a large variety in the diffusion coefficients of diffusing particles inside the same system (Figure 4.4).
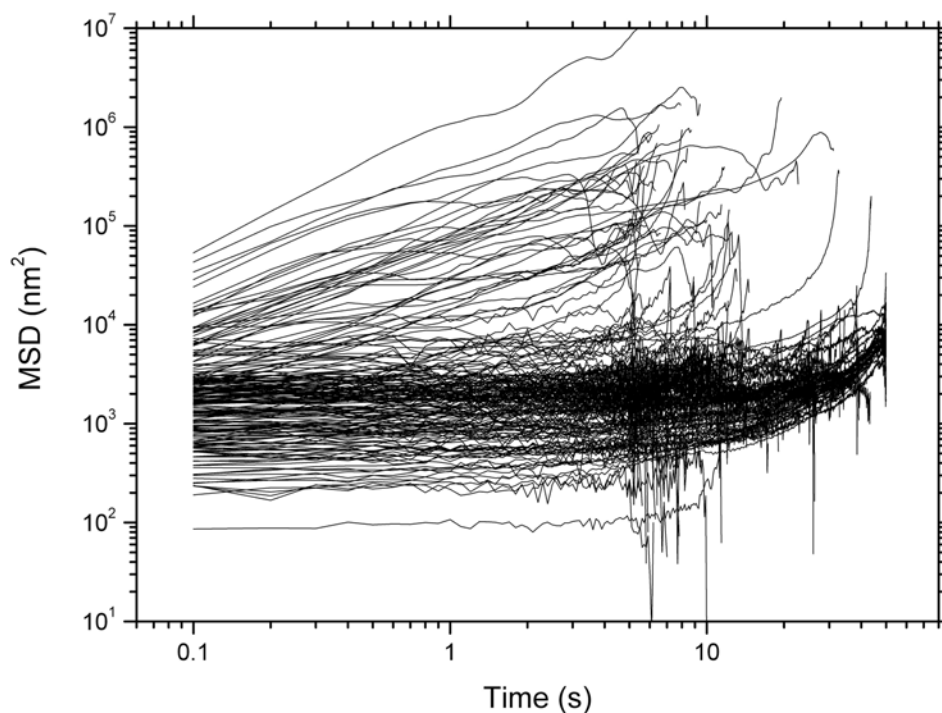
Figure 4.4 Semilog graph of MSD vs. τ of every diffusing single terrylene molecule.

The large variation in diffusion coefficients may be due to the defects in the prepared sample. The sample was not homogeneous everywhere. Although the overall expected morphology was obtained, there were some heterogeneities at some parts. Moreover, some of the molecules were making 2-dimensional Brownian motion while some of them were diffusing inside the cylindrical channels and some of them were immobile. All of these things result in different diffusion coefficients of the molecules. With this information in mind, individual trajectories in P2327 and P1945C were analyzed to differentiate the molecules which possessed different modes of motion.

In this study, the normal diffusion and sometimes the drifted diffusion of terrylene molecules were observed and focused on. The first examination was made by eye trying to check if the molecule could show a channeled diffusion. Then, the modes of selected trajectories were characterized by plotting the *MSD* curves as a function τ .

4.3 Analyzing Individual Trajectories in P2327 and P1945C Samples

In the following sections, the trajectory of the single molecules in annealed P2327 and P1945C samples with the AFM and SEM images of them are shown and discussed. There were several thousands of trajectories that were worked on but only some of them are discussed in detail since it is not possible to show all of them.

Terrylene molecules were embedded in PB-PEO polymer thin films and were used as probes. The motion of terrylene dyes in confined channels of a microphase separated block copolymer was investigated. As it is stated before, terrylene molecule is a hydrophobic fluorescent dye molecule and since the amorphous PB block of PB-PEO is also hydrophobic, it selectively went into the amorphous PB block due the hydrophobic interactions. The information about the structure is gained through the observation of probe molecule's diffusion inside the cylindrical channels of PB.

First, the individual trajectories which are diffusing inside the cylindrical channels of thin P2327 and P1945C films are discussed separately providing AFM and SEM images of them. And then, the molecules which confirm the presence of 1-dimensional channels in the plane of thick P2327 and P1945C films are presented. While doing this, some important features for understanding some additional information about the heterogeneities and defects are considered and some specific examples are shown. Moreover, the distribution of diffusion coefficient of the molecules in P2325 in addition to the distribution of them in P2327 and P1945C are discussed which would help for distinguishing P2327 and P1945C and for observing the confinement effect.

The trajectories of the single molecules in PB-PEO films in each section confirmed the presence of 1-dimensional channels in the plane of the film. For some specific cases, they also provided additional information about the heterogeneities and defects.

4.3.1 Results Obtained from Thin P2327 Film

4.3.1.1 AFM Results

The prepared P2327 sample was analyzed with AFM and SEM first to determine the surface morphology of it. Below, the AFM image of P2327 sample prepared from the solution containing 10 mg/mL P2327 doped with 15 nM terrylene after 6 hours of annealing is shown (Figure 4.5).
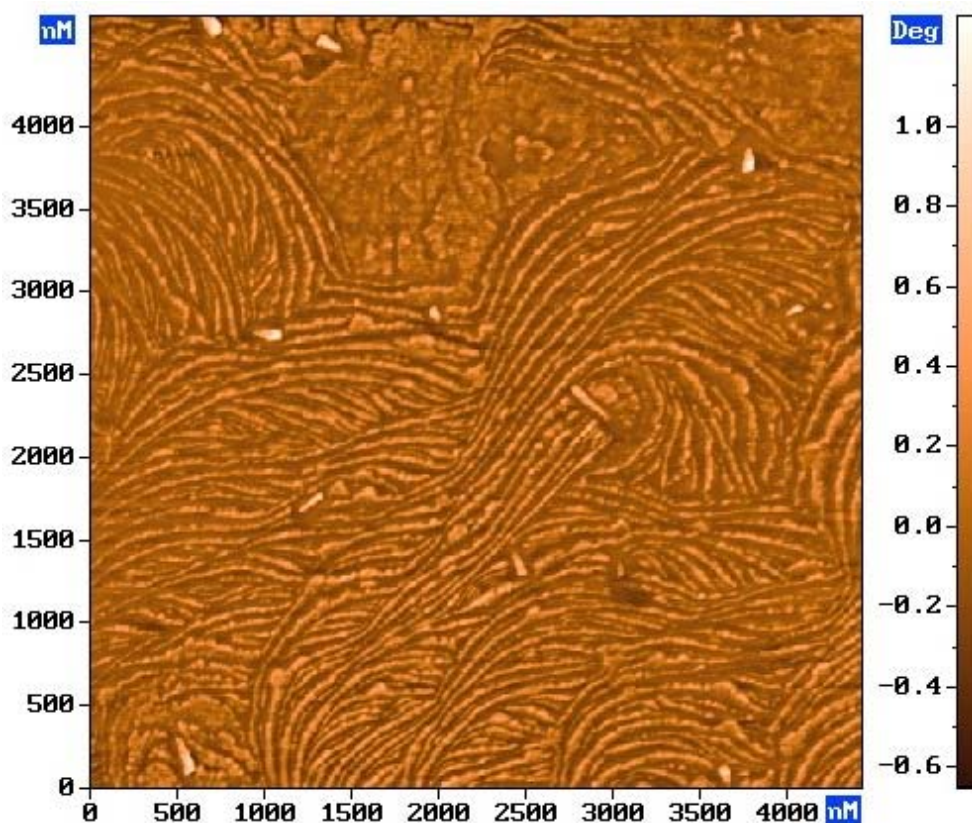
Figure 4.5 AFM phase image of thin P2327 film.

In this image, the dark lines correspond to PB channels where the brighter lines indicate the crystalline PEO blocks. The period of the self assembled morphology obtained for this sample was determined to be 59±1nm corresponding to an average PB channel diameter of 28 nm in the bulk. The hydrophilic PEO block prefers to be in touch with underlying glass substrate. As the presence of hydrophobic PB block at air/film interface lowers the interfacial energy, the PB channels are seen to be wider than the expected bulk diameter resulting in slightly wider channels. A film thickness may also allow a second layer of PB channels to be partially incorporated on top of the film as drawn in Figure 2.4.

It is also important to notice that the channels are not so much uniform in this film. There are some nonuniformities in channel diameters at some regions and also all the channels are not linear having some curved structures at some parts. This would affect the motion of single molecule.

4.3.1.2 SEM Results

Below the SEM image of thin P2327 film after 6 hours of annealing is shown.
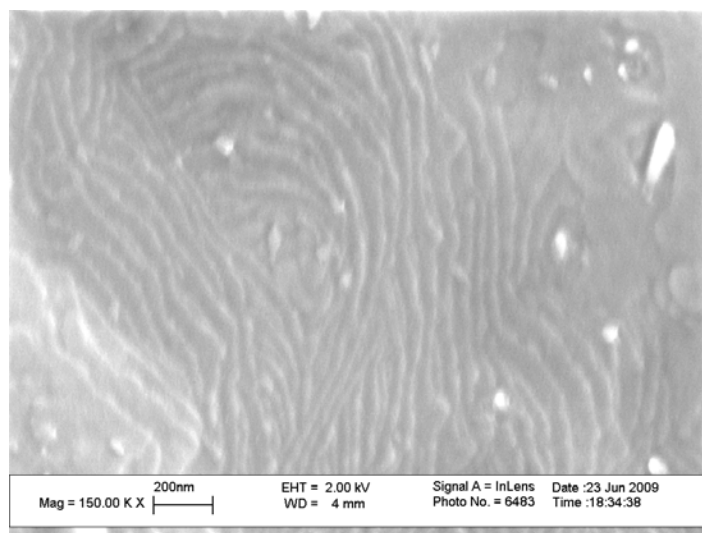
Figure 4.6 SEM image of thin P2327 film.

Here, the period of the self assembled morphology was measured to be around ~51 nm being consistent with the AFM results. This corresponds to an average PB channel diameter of ~24 nm in the bulk. In this SEM image, the curved channels and the increase in the channel widths are also seen verifying the observation about the nonuniformities on the sample obtained through AFM images.

4.3.1.3 Individual Trajectories Obtained from Thin P2327 Film

The average width of the trajectories indicating 1-dimensional channels remains around 25-60 nm while the molecules travel a contour length of 0.5-3.0 μm. The distribution of angles between two consecutive steps in almost linear trajectories, such as in figure 4.7a, is peaked at 0 and π rad, indicating the dominance of forward and backward steps in motion and confirming the 1-dimensional nature of the trajectories. The trajectory in Fig. 4.7b is an example of a curved single PB channel similar to those seen in the AFM and SEM picture of Fig.4.5 and Fig.4.6. Large variations were observed in step lengths at different parts of a given trajectory. These can be attributed to the presence of physical heterogeneities in the single channels such as variable channel diameter and local curvature, although the chemical heterogeneities in the channels cannot be ruled out. Figure 4.7c and 4.7d show the presence of nearly parallel channels. The molecules move from one channel to a neighboring channel due to the presence of defects in the film. These defects correspond to the disordered regions where the channels intersect as seen in Fig.4.5 and Fíg.4.6. Once the molecule reaches the defect, it is temporarily trapped and moves randomly until it enters one of the intersecting channels. This random motion disrupts the minima observed in angle distribution for motion in well-defined channels (Fig.4.7b lower inset) and results in a more uniform angle distribution. The 1D diffusion coefficients of the molecules were determined from the slope of mean square displacement vs. time graphs using $MSD(\tau) = 2D\tau$ [26, 31, 34]. For the molecules shown in Fig.4.7, diffusion

coefficients between 0.005-0.125 μm^2/s were measured. These values compare well to the
diffusion coefficients of different dye molecules in various mesoporous systems [42]. The
average of 1-dimensional diffusion coefficients of 48 molecules which were diffusing
inside thin P2327 film is 0.061μm^2/s.
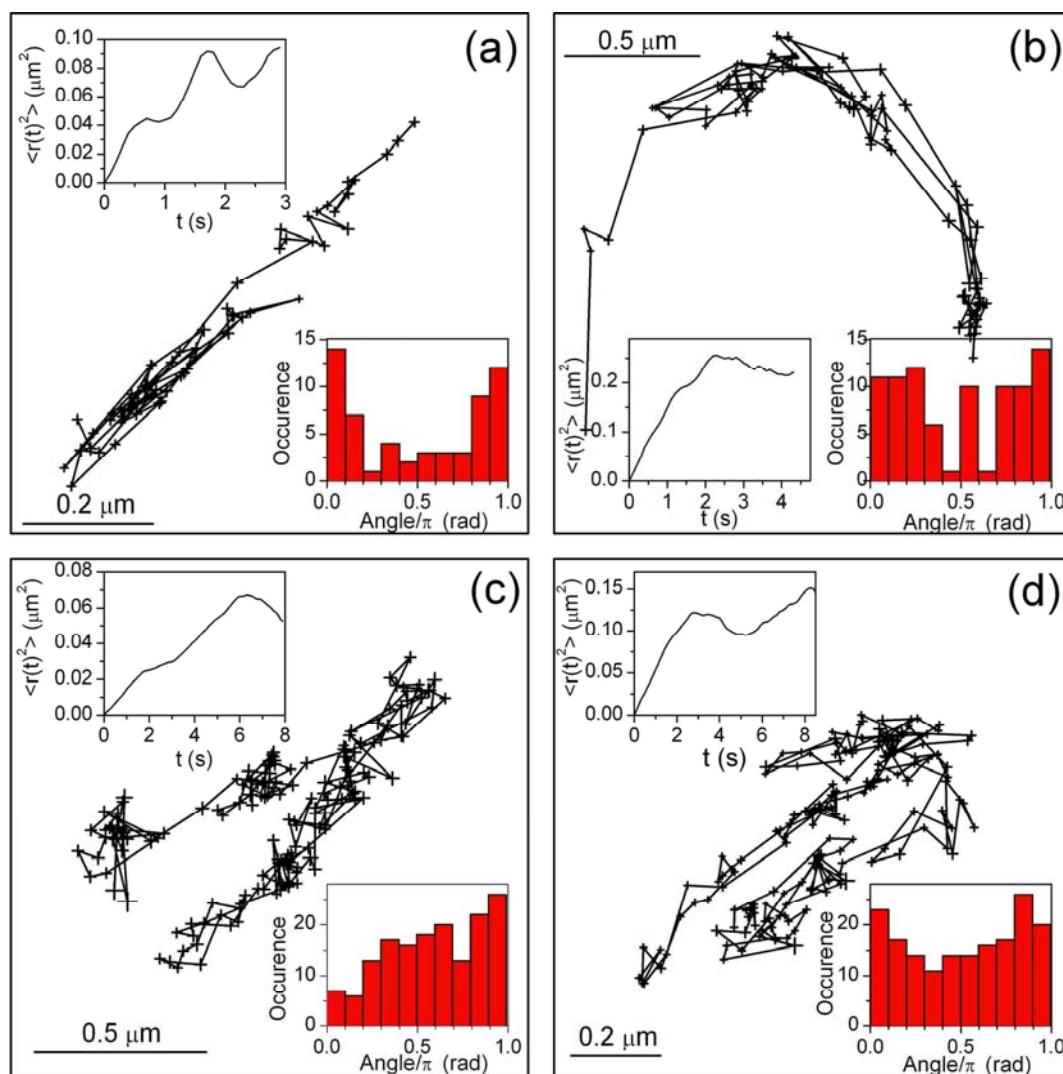
**Figure 4.7 Trajectories followed by four different single molecules in thin P2327 film. Error bars
indicate the localization accuracies at each step. Insets show the corresponding MSD vs. τ and angle
histograms.**

In addition to 1-dimensional normal single motion where $MSD(\tau)$ was proportional
to τ, directed single particle motion was also observed in the PB channels. In the following
figure, two different molecules possessing directed motion are presented. In theses images,
$MSD(\tau)$ vs. τ graphs exhibit directed motion showing the characteristic parabolic time
dependence and the trajectories and angle distributions of them are also included as insets.
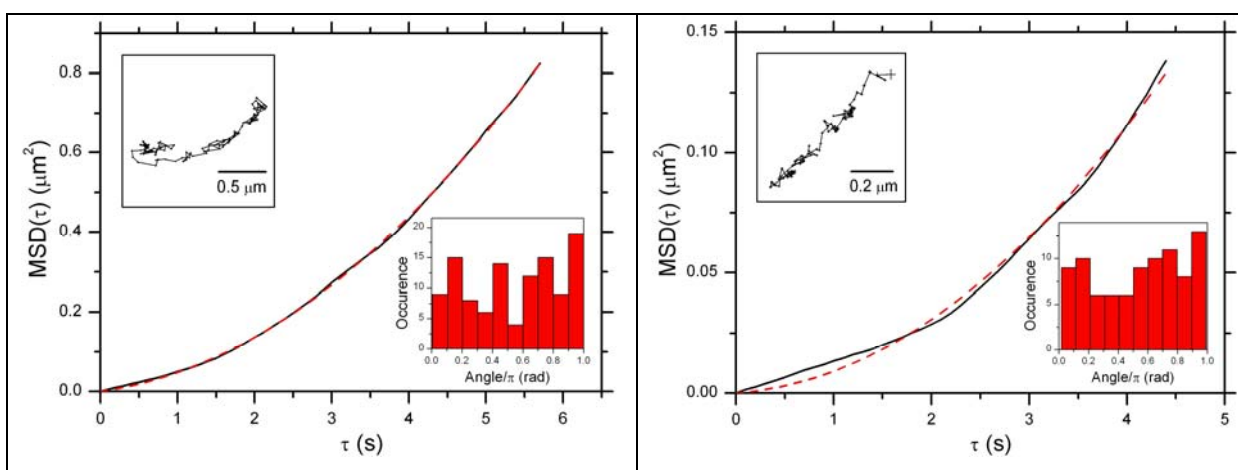
**Figure 4.8 Mean square displacements of single molecules exhibiting directed motion in thin P2327
film. Insets show the trajectory followed by the molecule and the corresponding angle histograms.**

The dashed lines are fits to the formula given by $MSD(\tau) = 2D\tau + (V\tau)^2$ with the best
fit parameters D=0.014 μm^2/s; V=0.14 μm/s and D=0.0014 μm^2/s; V=0.079 μm/s for the
left and right images, respectively. A frame by frame examination of the trajectories of
directed motion shows that the molecules are moving in forward direction preferentially.
For instance, longer steps are observed in forward direction whereas the steps sizes are
smaller in the backward direction. Such motion can be explained by the non-uniformity of
the PB channels which might be observed due to the effect of film/substrate and air/film
interfaces. With increasing channel widths that are observed in the AFM images also, the
average mean free path of a single molecule is expected to increase and the local density in

the channels expected to decrease. So, these effects might tend to direct the motion of probe molecules in the direction of increasing channel width.

There were also such molecules showing some complicated diffusion. For instance, the molecules whose results are shown in the following image starts its motion doing some random walk and after that it shows some backward and forward movement at some parts of its motion indicating the 1-dimensional diffusion. So, this type of motion also proves the presence of some defects on the sample which could not be ruled out chemically in detail.
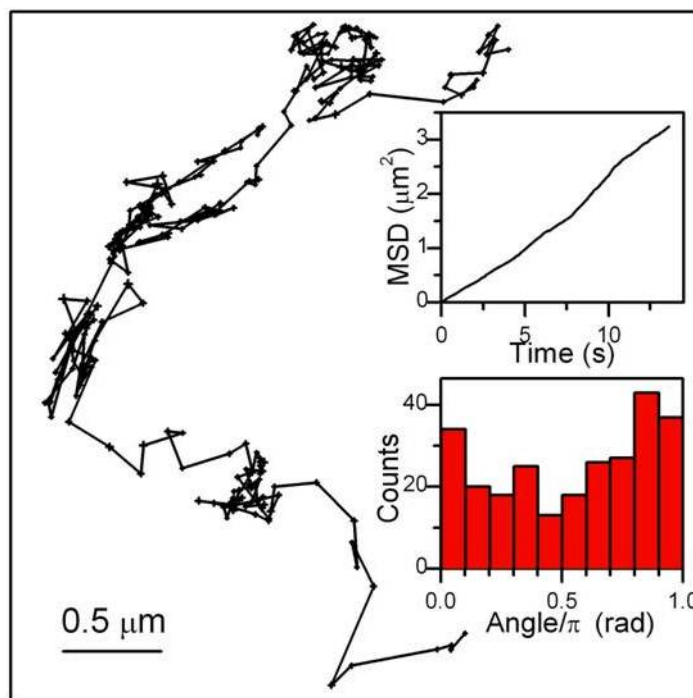
Figure 4.9 A single terrylene molecule showing a complicated type of motion doing random walk at some parts and 1-dimensional diffusion at other parts is. Insets show the MSD(τ) vs. τ graph and the angle histogram.

4.3.2 Results Obtained from Thin P1945C Film

4.3.2.1 AFM Results

Below, the AFM phase image of thin P1945C film after 6 hours of annealing is shown.
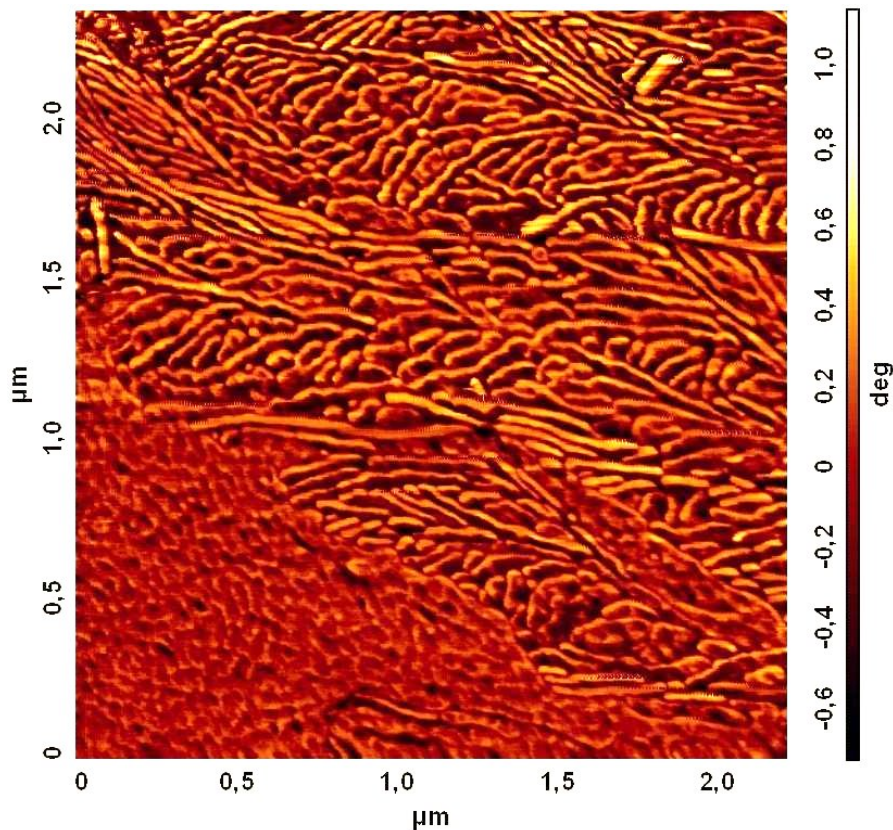
Figure 4.10 AFM phase images of thin P1945C film.

The dark lines again correspond to the PB channels where the brighter lines show the PEO crystalline blocks. The period of the self assembled morphology obtained from 10mg/mL P1945C was determined to be 26±1nm corresponding to an average PB channel diameter of 12.3 nm in the bulk. In the film, linear channels which are intersecting each other are mostly present. The lengths of the formed channels are ranging between 90 nm

and 0.7 μm where most of the channels fall in the group of short channels. There is no significant curved channel. However, there are some PB regions blocked by PEO crystalline parts which don't have significant shape. They can behave just like some traps for the molecules diffusing inside them. So, these PB regions would let the molecules to make confined motion in them. Also parallel channels ending at the same open point are present which would let the molecule to switch between them.

4.3.2.2 Individual Trajectories Obtained from Thin P1945C Film

The trajectories of single terrylene molecules inside 1-dimensional channels of PB are shown in figure 4.11. In figure 4.11b, the back and forth movement of the molecule is clearly observable from the trajectory which makes the angle histogram meaningful peaking at 0 and π radian showing the presence of 1-dimensional channel. In figure 4.11a, after watching the movie of the diffusing molecule, we are sure that the molecule is inside the channel of PB. However, its angle histogram is disrupted which can be attributed some disordered regions inside the channels. In figure 4.11c and 4.11d, the switching of the molecules between parallel neighboring channels is observed through some open regions at the intersection point of the channels. The angle histograms are peaked at 0 and π radian resulting from the 1-dimensional movement of the molecule. The minimum width observed from the trajectories was around ~25 nm which ranges up to 140 nm. Observation of 140 nm width of a channel makes sense when the molecule moves inside the parallel channels switching between them. The average contour length traveled by a molecule was between 0.25-2.5 μm. As the maximum channel length observed by the AFM image was 0.7 μm, the molecules have to continue their motion inside another nearer channel when the length of the channel that they were present was not long enough. The average 1-dimensional diffusion coefficient of 35 molecules which were diffusing inside thin P1945C film is found to be 0.040 μm^2/s.

**Figure 4.11 Trajectories followed by four different single molecules in thin P1945C film. Insets
show the corresponding MSD vs. τ and angle histograms.**

4.3.3 Comparison of the Results Obtained from Thin P2327 and P1945C Films

It is possible to compare the results of P2327 and P1945C samples obtained from the
single molecule measurements since the concentrations of the dye solution and polymer
solution are kept same. When the trajectories are observed and analyzed, they confirm the
topology observed through AFM and SEM images such that curved, parallel and linear
motion are observed from the trajectories of single molecules in P2327 whereas only
parallel and linear motion are observed in P1945C. Moreover, we claim that while keeping
the volume fraction of PB (PEO) constant of about 0.20 (0.80), changing the molecular
weight of the diblock copolymer PB-PEO having the same molecular structure changes the
radius of the formed cylindrical channel. This is consistent with the AFM results where the
diameters of PB channels are 28 nm and 12.3 nm for the films prepared from 10 mg/mL
P2327 and P1945C, respectively. So, the two polymer system can be separated through the
distribution of diffusion coefficient of single molecules moving inside the channels of them
since the expected channel diameter of PB in P2327 is larger than the channel the channel
diameter of PB in P1945C. The average 1-dimensional diffusion coefficient of 48 terrylene
molecules in P2327 is $0.061 \mu m^2$/s where it is 0.040 μm^2/s for 35 molecules in P1945C
being consistent with the expected results. Differentiating of the two polymer system
statistically is also possible. When the histograms of the 1-dimensional diffusion
coefficients are plotted for both P2327 and P1945C, the dominance of larger diffusion
coefficients after 0.07 μm^2/s is observed for P2327 as seen in the following figure (Figure
4.12).
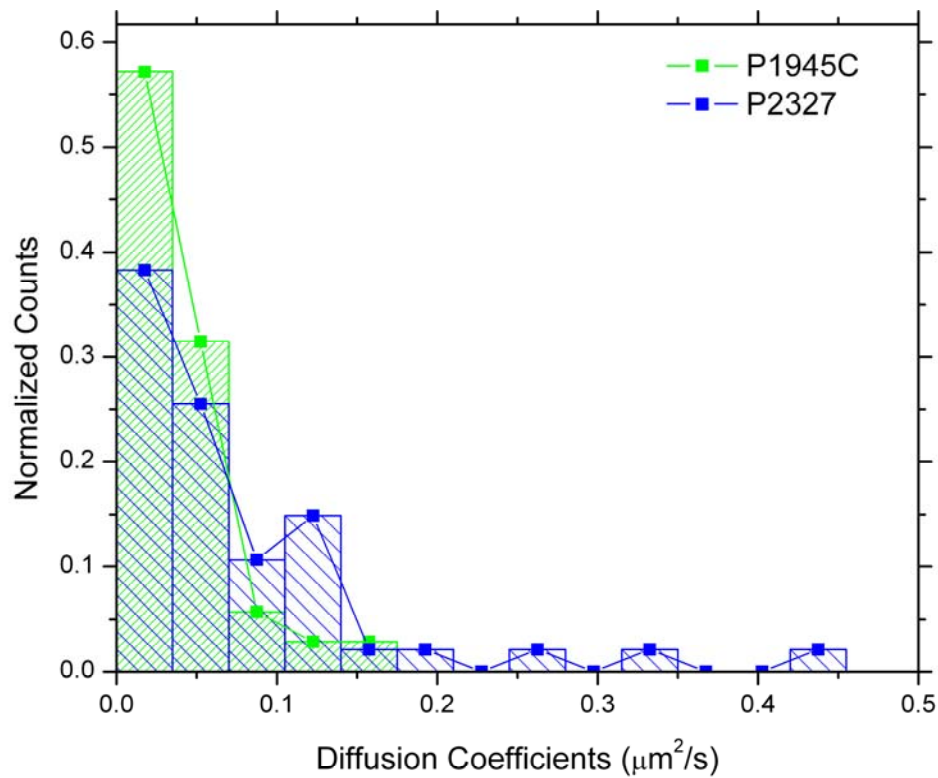
Figure 4.12 The normalized histogram of diffusion coefficients of single terrylene molecules in 1-dimensional PB channels of thin P2327 and P1945C films.

4.3.4 Results Obtained from Thick P2327 Film

4.3.4.1 AFM Results

Below, the AFM image of thick P2327 film is shown (Figure 4.13).
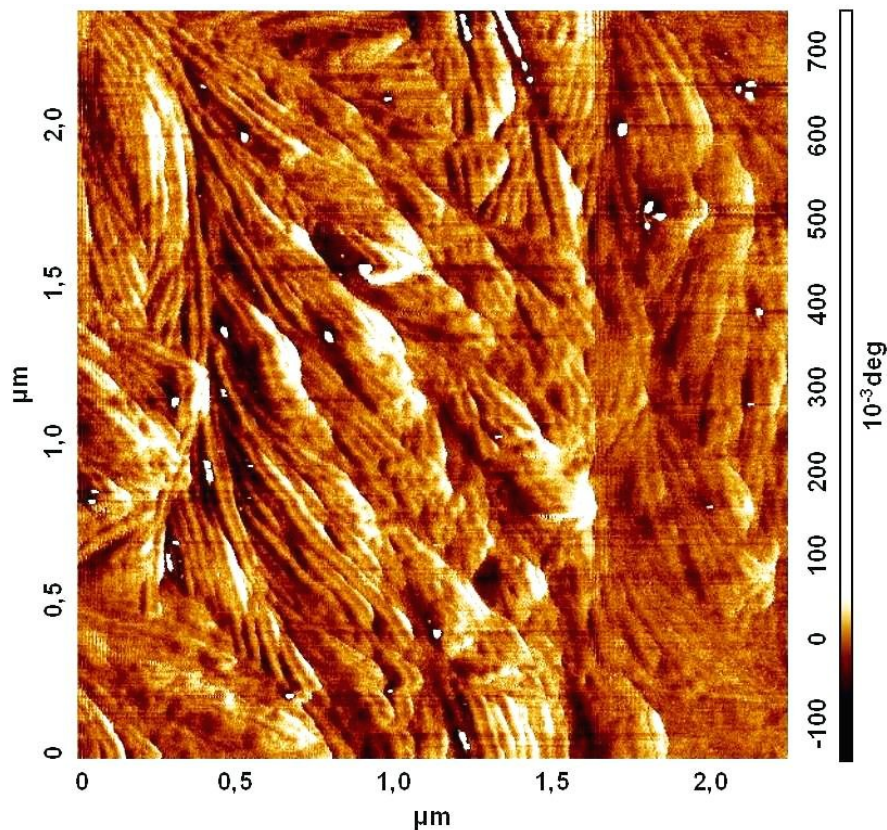
Figure 4.13 AFM phase image of thick P2327 film.

In this film, the period of the self-assembled morphology is determined to be 48±1nm corresponding to an average PB channel diameter of 22.8 nm in the bulk. The thickness of this film is expected to be two fold of the thin P2327 film allowing a few more layers of PB channels.

4.3.4.2 Individual Trajectories Obtained from Thick P2327 Film

Parallel and curved channels are still observed in addition to single linear channels as expected from the morphology obtained. However, while doing analysis, finding trajectories which show 1-D diffusion was difficult. The average diffusion coefficient of 45 molecules moving inside the channels is calculated as 0.120 μm^2/s which is higher than the average diffusion coefficient of terrylene molecules inside low molecular weight P2327 sample. In fact, we expect them to be at similar values. This is because the diameters of the observed channels from AFM images are comparable. So, there should be some surface effect which should be worked out. Meanwhile, the channel widths measured from the trajectories are wider ranging between 33 nm and 103 nm. So, while they are moving along the channels, they may be switching between each other which would lead the molecule to diffuse as doing 2-dimensional diffusion. The molecules shown in figure 4.14a and 4.14b diffuses along one straight channel with diffusion coefficients of 0.051 μm^2/s and 0.031 μm^2/s, respectively. Parallel channels and curved channels were also observed as shown in figure 4.14c and 4.14d. In figure 4.14c, the molecule changes its pathway to another channel while it is moving along other straight channels through some defect. Its diffusion coefficient is calculated to be 0.029 μm^2/s. Lastly, curved channels as observed in the AFM images could be detected as shown in figure 4.14d. The angle histograms of these molecules which are shown at lower insets were generally peaked at 0 and pi radian. However, uniform distribution was also observed due to some defects in the channel formation since it leads the molecule to make movement different from perfect linear motion.
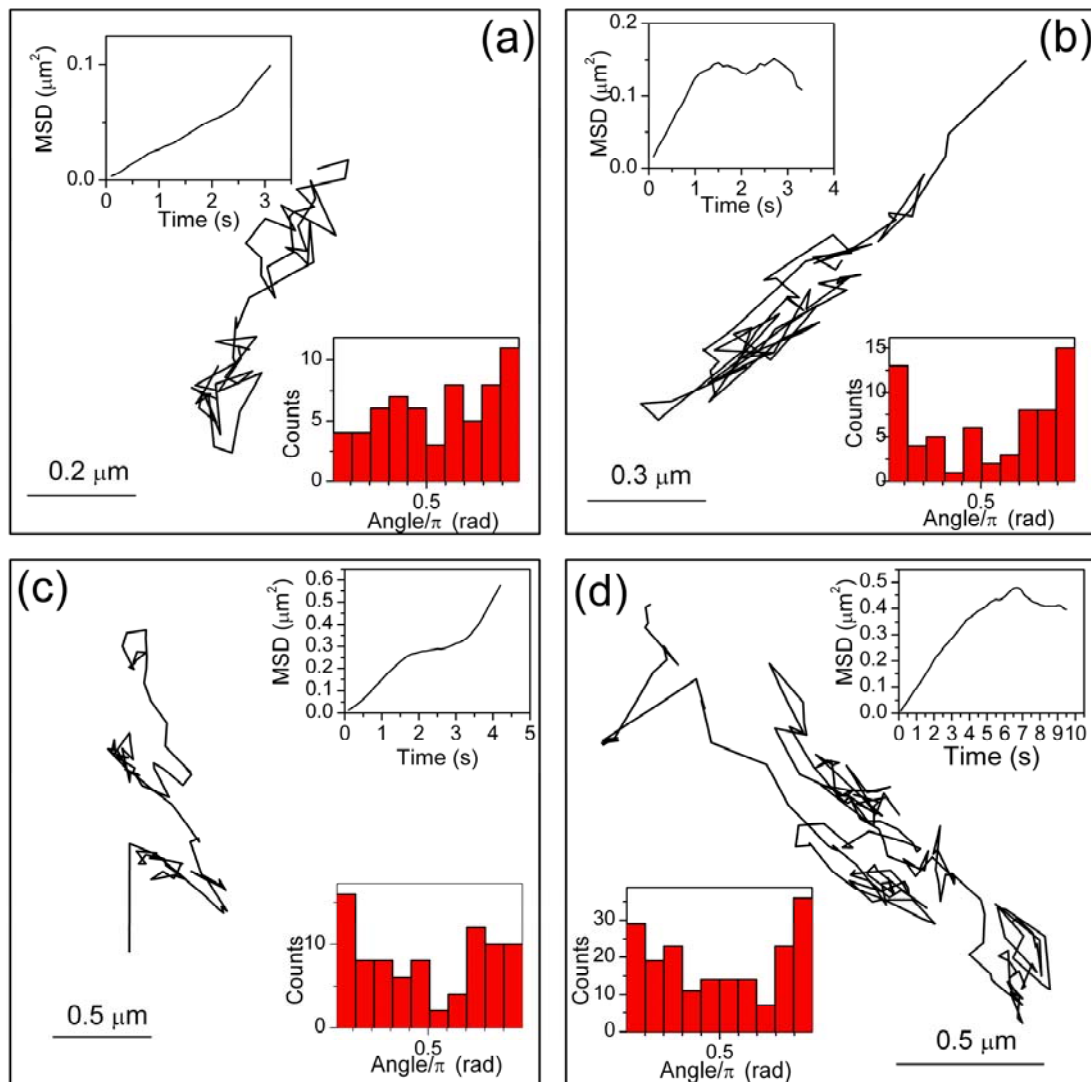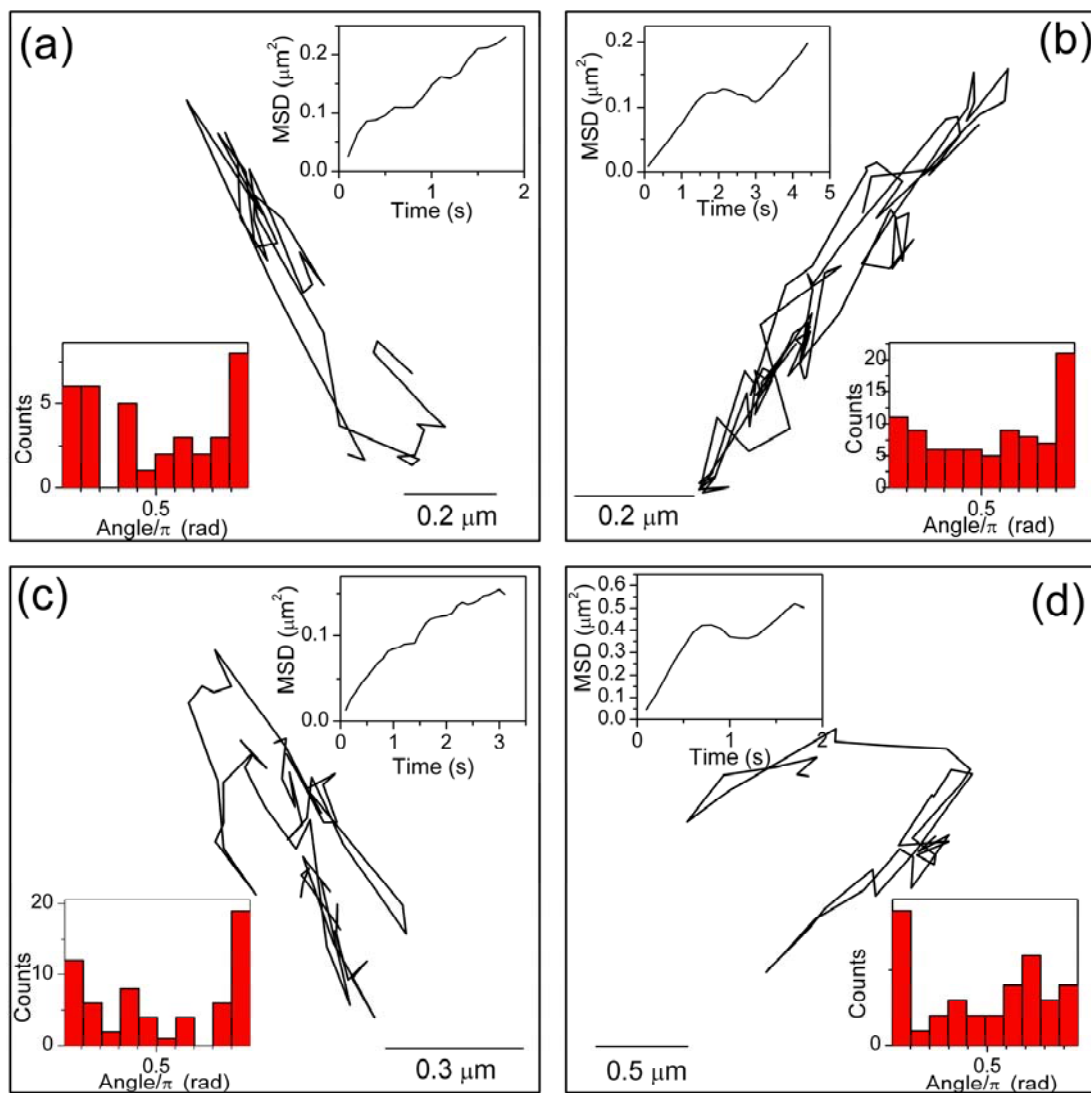
Figure 4.14 Trajectories followed by four different single molecules in thick P2327 film. Insets show the corresponding MSD vs. τ and angle histograms.

In addition to normal diffusion of terrylene molecules in thick P2327 film, directed
diffusion of them were also observed due to some probable reasons that are discussed in
section 4.3.1.3.
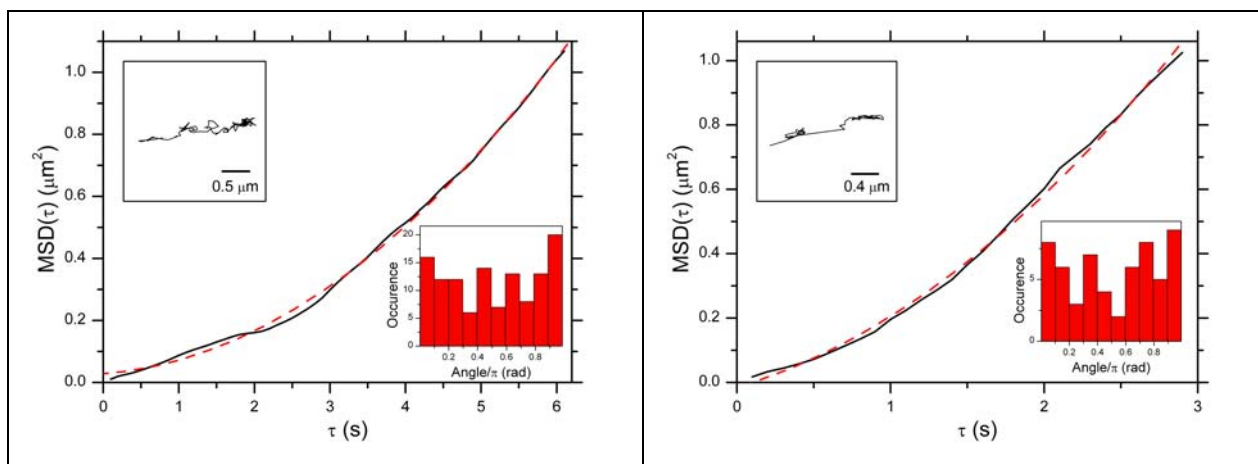
**Figure 4.15 Mean square displacements of single molecules exhibiting directed motion in thick P2327
film. Insets show the trajectory followed by the molecule and the corresponding angle histogram.**

For the left and right one, the diffusion coefficients and drift velocities are calculated as
D=0.00952μm^2/s; V= 0.158μm/s and D=0.07084μm^2/s; V=0.281μm/s by fitting the lines to
the formula given by $MSD(\tau) = 2D\tau + (V\tau)^2$, respectively.

4.3.5 Results Obtained from Thick P1945C Film

4.3.5.1 AFM Results

The AFM image of the thick P1945C film is shown in figure 4.16.
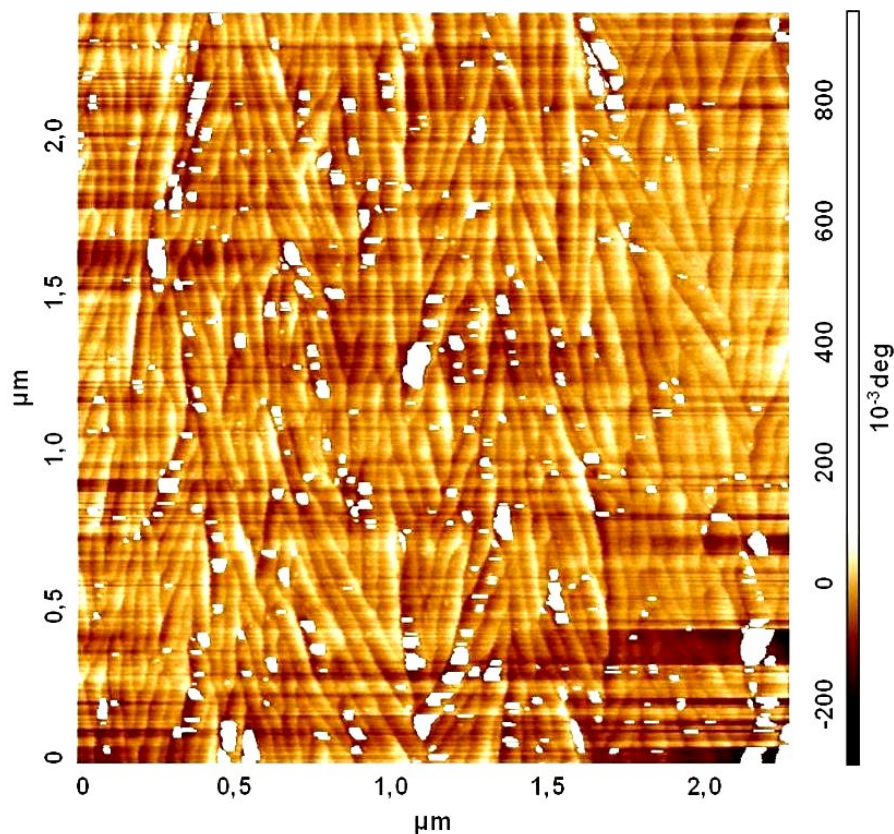
Figure 4.16 AFM phase image of thick P1945C film.

Here, the self-assembled morphology is 45±1nm corresponding to 21.5nm channel diameter of PB in the bulk. The formed cylindrical channels in this film are linear. They are long with respect to the film of 10 mg/mL. There seem some overformed channels on the other channels of PB since the thickness of the film is two fold of the thin P1945C film. There are no curved channels and a few parallel channels ending at the same open

amorphous PB region. So, observation of curved motion is not expected or where switching
of the molecule between parallel channels may be observed.

4.3.5.2 SEM Results

Below the SEM image of thick P1945C film after 6 hours of annealing is shown (Figure
4.17).
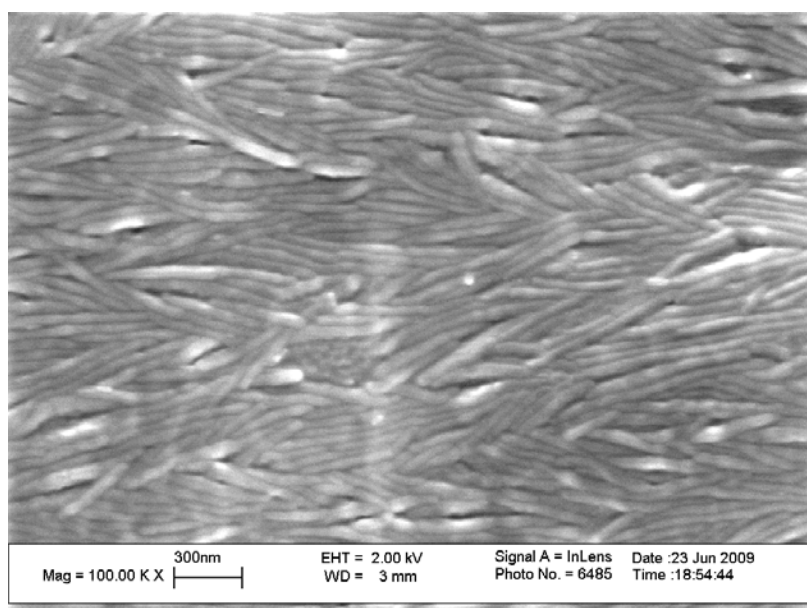
Figure 4.17 SEM image of thick P1945C film.

In this sample, the period of the self assembled morphology was measured to be around
~46 nm being consistent with the AFM results. This corresponds to an average PB channel
diameter of ~22 nm in the bulk. Through this SEM image, the presence of parallel long
linear channels is verified which is also observed in AFM image.

4.3.5.3 Individual Trajectories Obtained from Thick P1945C Film

Trajectories obtained from single molecule techniques were really good. Linearity was observed in all of them. Angle histograms were really convincing about the presence of 1-dimensional channels. Molecules switching between parallel channels were present. Below, there are four figures selected among 50 of them.
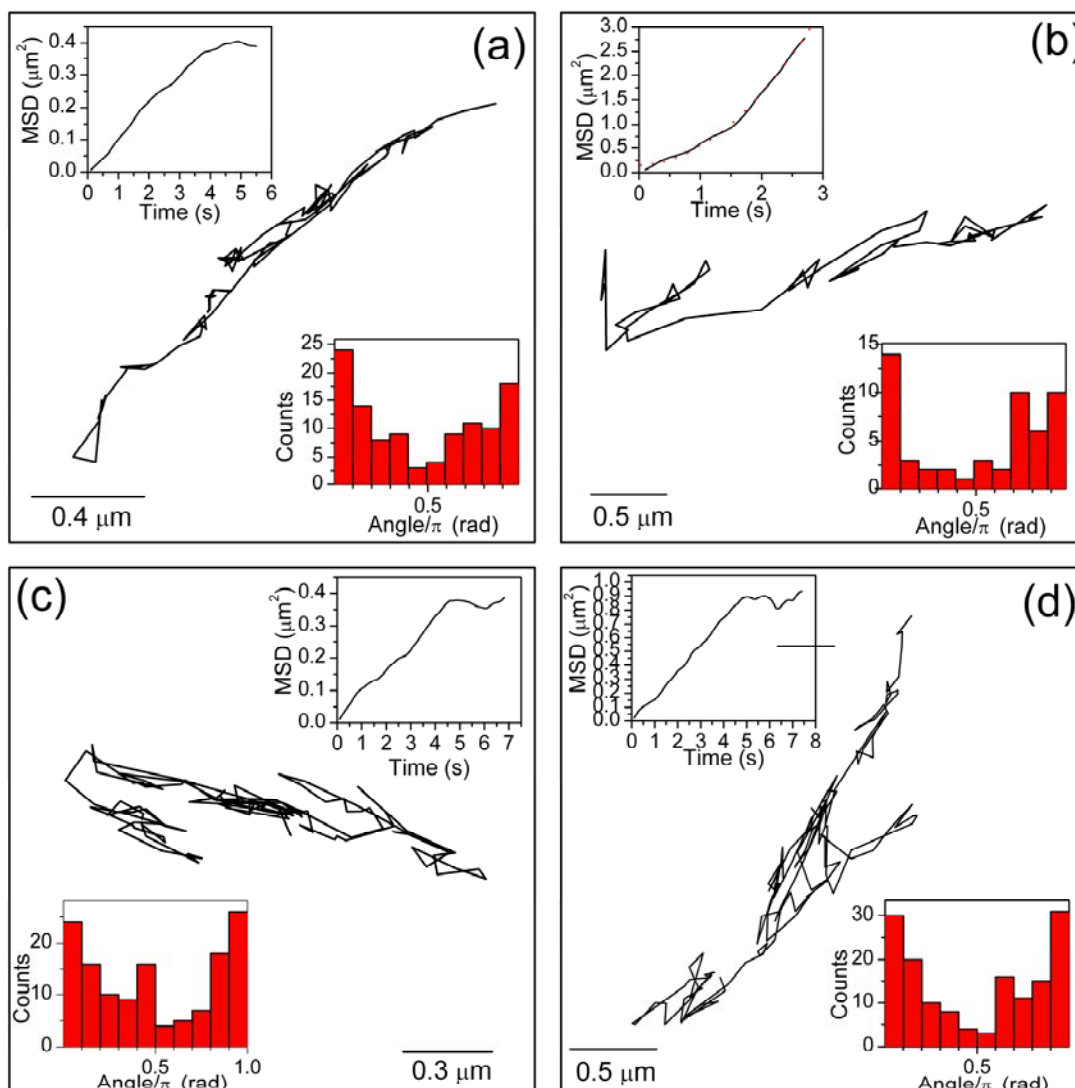
Figure 4.18 Single molecule trajectories in thick P1945C film. Insets show the corresponding MSD vs. τ and angle histograms.

The average diffusion coefficient of these 50 molecules is calculated as 0.134 μm^2/s. In figure 4.18a, the trajectory of a diffusing molecule in a very narrow and straight line is shown. Here, the presence of long and straight channel is very well presented. The diffusion coefficient of this molecule is calculated as 0.055 μm^2/s inside 24 nm width channel. The molecule shown in figure 4.18b is similar to those that are shown in previous sections making directed diffusion in the sense of *MSD* calculation. However, this molecule also shows some parallel channels while its diffusion with drift. Its diffusion coefficient is 0.032 μm^2/s with drifting velocity of 0.583 μm/s. This molecule starts its motion going along and inside one long channel and some later time of its diffusion, going along small channels and returning along the same way is observed 3 different parts. So, calculation of different channel width at different parts of this molecule's trajectory was possible and channel widths ranging between 21 nm and 56 nm was observed. The molecule apparently switching between parallel channels having channel widths between 40-75 nm is shown in figure 4.18c. There were three parallel channels shown in this figure.

4.3.6 Comparison of the Results Obtained from Thick P2327 and P1945C Films

It was difficult to separate the two samples by looking at the distribution of their diffusion coefficients. Although diffusion coefficients of the molecules inside thick P2327 film were larger than in thick P1945C film after 0.3 μm^2/s, the dominance of diffusion coefficients of molecules inside thick P1945C film falling into 0.2 μm^2/s - 0.3 μm^2/s range makes it difficult to differentiate these two samples looking at their diffusion coefficient histograms. This conclusion also makes sense when we look at the average diffusion coefficients of molecules inside the thick films of P2327 and P1945C which are 0.120 μm^2/s and 0.134 μm^2/s, respectively. However, these obtained results can be expected remembering the AFM and SEM results of the samples. The calculated channel widths for thick P2327 and P1945C films are 22.8nm and 22 nm, respectively although these are not

the intended results. The reason behind having such larger channel widths in thick P1945C film can only be explained by the following: The PB cylindrical channels might have overspread at upper parts of the sample without being able to preserve its cylindrical shape due to the lower surface energy of PB and the usage of high concentration P1945C which has smaller molecular weight.

Figure 4.19 The normalized histogram of diffusion coefficients of single terrylene molecules in 1-dimensional PB channels of thick P2327 and P1945C films.

4.4 Analyzing Individual Trajectories in P2325 Film

In addition to 1-dimensional normal single particle motion, 2-dimensional diffusion of them where $MSD(\tau)$ was proportional to τ was also observed. Very thin film (film thickness ~27nm) of P2325 diblock copolymer showing lamellar morphology in the bulk was utilized for this purpose. In the film, PEO part is expected to be formed on hydrophilic glass substrate where 2-dimensional PB layer is formed on top of PEO layer at the air/film interface. To be sure that the PB layer is on top at the air/film interface, we measured the contact angle of water drops on the film and it was larger than 90° meeting our expectations. The thickness of the PB layer is expected to be ~13nm as the volume fraction of PB is 0.49.

The diffusion coefficients of 136 different terrylene molecules exhibiting 2-dimensional diffusion in ~13nm thick top PB layer are calculated. The average 2-dimensional diffusion coefficient of 136 molecules is calculated as 0.112 μm^2/s. Below, two molecules are shown as examples for molecules exhibiting 2-dimensional diffusion (Figure 4.20). In figure 4.20a and 4.20b, the trajectories of molecules are seen at top left corners, angle historgrams are seen at right top corners and MSD calculations as a function of time and linear fits to them are shown at the bottom parts of these figures. In the trajectories, the random motion of single molecules is clear. The uniform distribution in angle histograms and the proportionality of $MSD(\tau)$ to τ are also clearly demonstrating the presence of 2-dimensional diffusion.
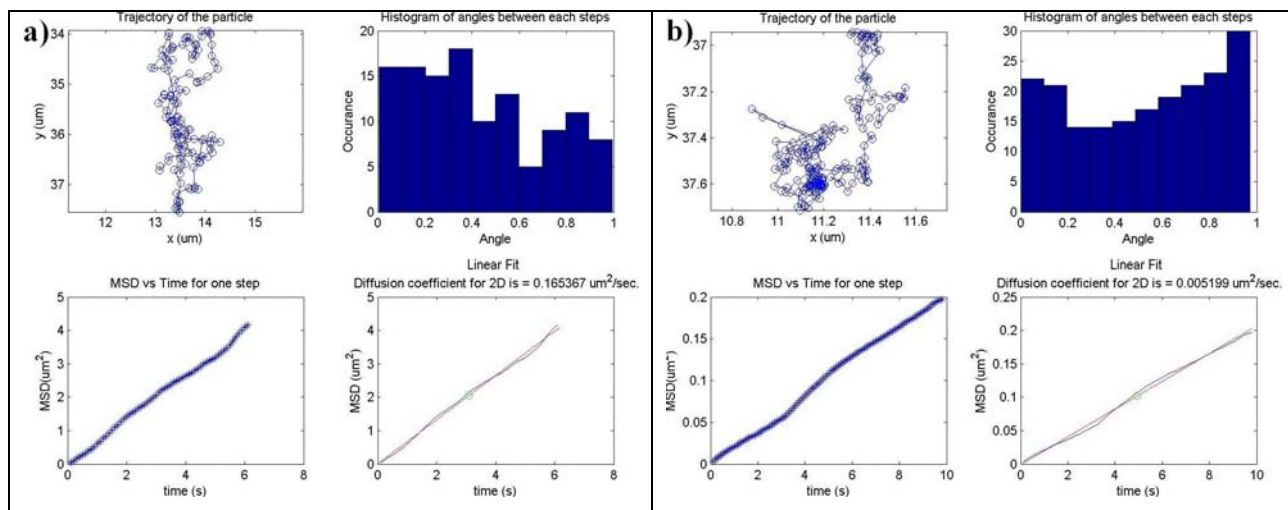
Figure 4.20 Trajectories of two terrylene molecules showing 2-dimensional diffusion with their angle histogram, MSD(τ) vs. τ graph and linear fit to MSD(τ) vs. τ for determining their diffusion coefficients.

4.4.1 Comparison of the Diffusion Coefficients in Thin and Thick P2327 and P1945C Films with Diffusion Coefficients in P2325 Film

The histogram of diffusion coefficients of 136 molecule exhibiting 2-dimensional diffusion is plotted for comparison with diffusion coefficient histograms of molecules in 4 different samples that are discussed in previous sections. First, the histogram of 2-dimensional diffusion coefficients are compared with 1-dimensional diffusion coefficients in thin P2327 and P1945C films. Then, this comparison is made using the results obtained from thick P2327 and P1945C films.

A significant difference between 1- and 2-dimensional diffusion coefficients was observed for diffusion coefficients larger than $0.15\mu m^2$/s as seen in figure 4.21. 2-dimensional diffusion coefficients ranged up to $1\mu m^2$/s being ~3 times larger than the range of those 1-dimensional diffusion coefficients. This difference could also be observed through their average diffusion coefficients which are $0.040\ \mu m^2$/s, $0.061\mu m^2$/s and $0.112\ \mu m^2$/s for thin P1945C film, thin P2327 film and P2325 film, respectively.
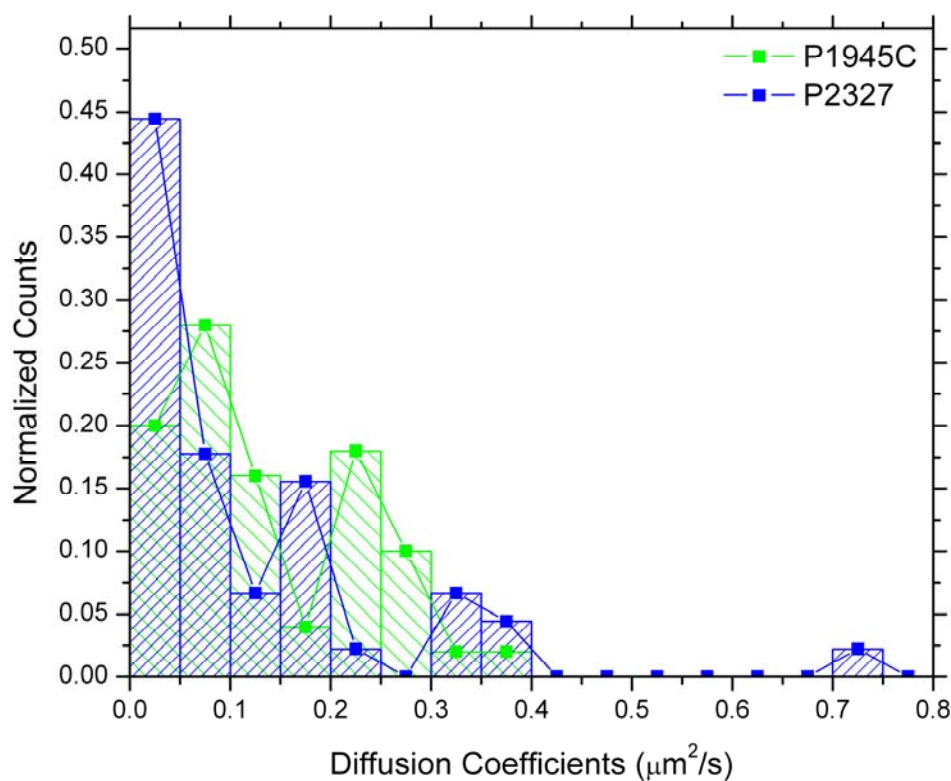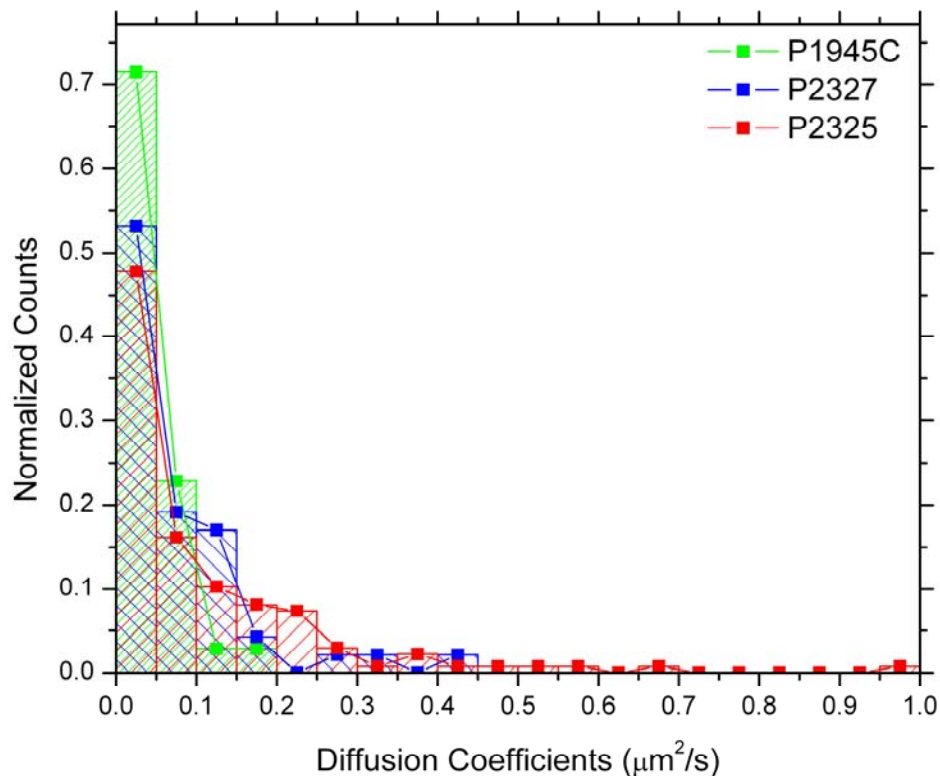
Figure 4.21 The normalized histogram of diffusion coefficients of single terrylene molecules in 1-dimensional PB channels of thin P2327 and P1945C films and 2-dimensional layer of P2325 film.

For results obtained from thick P2327 and P1945C films and P2325 film, it is difficult to say that there is a significant dominance of 2-dimensional diffusion coefficients at larger diffusion coefficients (Figure 4.22). This can be due to the same reason that is discussed in section 4.3.6. The average diffusion coefficients of them were also similar being 0.134μm^2/s, 0.120μm^2/s and 0.112 μm^2/s for thick P1945C film, thick P2327 film and P2325 film, respectively.
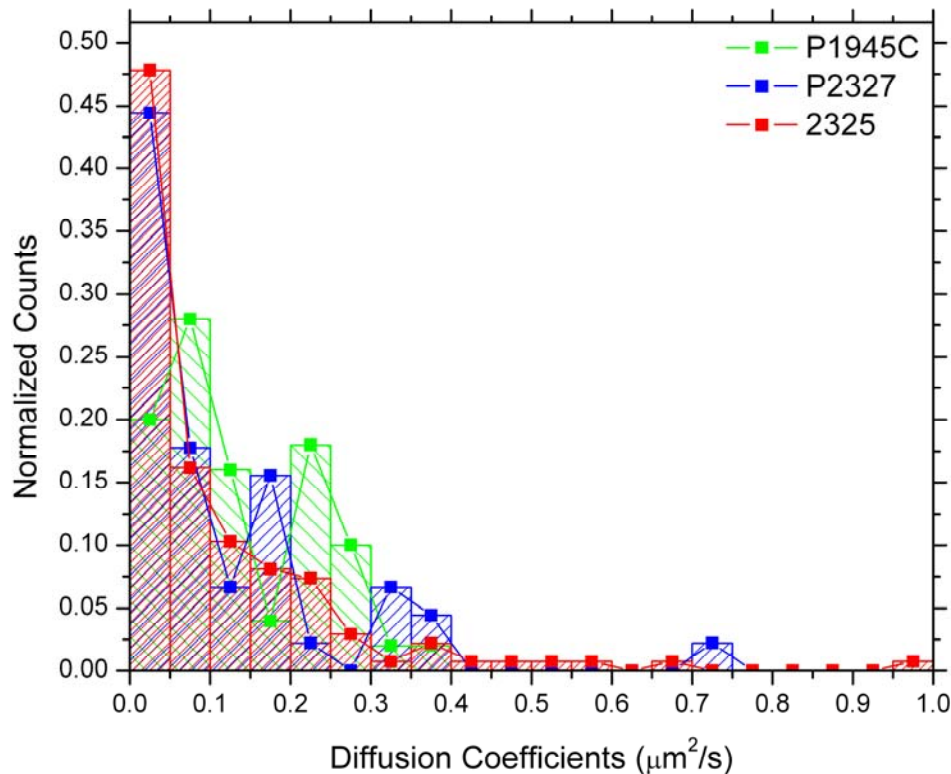
**Figure 4.22 The normalized histogram of diffusion coefficients of single terrylene molecules in 1-
dimensional PB channels of thick P2327 and P1945C films and 2-dimensional layer of P2325 film.**

4.5 Summary

The 1-dimensional diffusion of terrylene molecules is observed in cylindrical channels
of amorphous minor component PB inside the crystalline major component PEO. Directed
diffusion as well as the normal diffusion of single terrylene molecules were observed. The
likely origin for the directed diffusion of single molecules is discussed in terms of local
variations in the PB channel width and the resulting change in the local intensity. The non-
uniformities and the heterogeneities in motion were tried to be understood and related to
the inhomogeneities of the surface. Furthermore, different molecular weight polymers are

compared. The confinement effect is clearly observed for both thin and thick P1945C and P2327 films.

So, through the obtained results, it is shown that the single molecule tracking provides detailed understanding about the diffusion process and the host. By this way, single molecule tracking is very sensitive in characterizing the self-assembled block copolymer morphologies.

Chapter 5

CONCLUSIONS

After providing the necessary information for single molecule detection using TIRF microscopy technique at room temperature, we presented the materials and methods that we utilized through our experiments. Firstly, we dealt with characterization of single molecules. This was important since observation of some scattering rather than fluorescence is possible. It was needed to observe the characteristic behavior of single molecules for convincing ourselves about observing real fluorescence of single molecules and we could show the blinking and photobleaching of rhodamine B and terrylene molecules in PMMA and PS host materials, respectively. Then, defining the limitations of our experimental setup was essential since geometries that we obtained were in tens of nanometers range. So, we needed to make sure that we could study the dynamics of single molecules inside the obtained confined geometries on different PB-PEO diblock copolymer samples. We showed ~1.5 nm resolution in positioning both rhodamine B and terrylene molecules using our experimental setup in again PMMA and PS samples, respectively.

After providing this preliminary knowledge and results, we reported on the dynamic motion of single terrylene molecules inside 1-dimensional channels of PB with two different channels widths inside PEO matrix and in 2-dimensional layer of PB on top of PEO at air-film interface obtained from asymmetric and symmetric PB-PEO diblock copolymers, respectively.

We obtained the cylindrical channels inside thin and thick films of P2327 with channels diameters of 28 nm and 22.8 nm according to the AFM phase images, respectively. The AFM and SEM images of thin P2327 sample were also consistent with each other. We observed linear, parallel and curved channels through the trajectories of single molecules being consistent with the AFM and SEM results. The chemical reason behind obtaining different channel diameters with the same diblock copolymer could not be ruled out and should be worked on in future. The single molecule experiments might give useful information about this result if more experiments were performed. Moreover, directed diffusion of single molecules which was attributed to the increase in channel widths tending to increase the mean free path of single molecules and to decrease the local density at some regions on the sample surface was observed providing the information about the presence of non-uniformity in the PB channel.

The confined 1-dimensional cylindrical geometries were also well formed using P1945C for obtaining thin and thick films. However, problem with having comparable channel diameters on these two samples still continued. The channel diameters of PB were 12.3 nm and 21.5 nm for thin and thick films of P1945C according to the AFM phase images, respectively. The AFM and SEM images of thick P1945C sample were again consistent with each other. Nevertheless, the trajectories of single terrylene molecules gave detailed information about the morphologies of prepared samples. Only linear and parallel channels were observed being consistent with the AFM and SEM results. The only unexpected results were the observation of directed diffusion in thick film of P1945C in which the physical and chemical reasons should be worked out.

By the comparison of diffusion coefficient histograms of terrylene molecules in thin films of P1945C and P2327, it was possible to separate these two samples since the

dominance of larger diffusion coefficients of P2327 was clear. This conclusion was also consistent with average diffusion coefficients of terrylene molecules which were 0.040 μm^2/s and 0.061 μm^2/s for diffusing single molecules in 1-dimensional channels of P1945C and P2327 samples, respectively. On the other hand, it was difficult to differentiate thick films of P1945C and P2327 using single molecule experiment results which might be due to obtaining comparable channels diameters in both samples. However, this should be focused on in future preparing the samples of thick P1945C and P2327 samples and performing single molecule experiments, again.

Obtaining very thin films (27 nm) of P2325 in which the PB layer was formed parallel to the substrate on top of PEO layer at air interface allowed us to study the 2-dimensional diffusion of terrylene molecules. When we compared the results with 1-dimensional diffusion, we observed the confinement effect of single terrylene molecules in 1-dimensional confined geometries for both thin and thick films.

In the light of this evidence, the single molecule techniques gave detailed information on dynamic properties of probe molecules such as molecule's trajectory and their diffusivity inside the channels. We observed various trajectories depending on the morphology obtained. We could also investigate the details of geometrical features of nanosized confined spaces highlighting the sensitivity of single molecules to the non-uniformities and heterogeneities in the channels. The confinement effect in obtaining 1-dimensional channels was also investigated by comparison of 1-and 2- dimensional diffusion coefficient distributions.

These studies may contribute to future efforts to achieve long range order in self-assembled block copolymers and may be applied to other systems such as other porous

systems and biological membranes for their characterization since there is potential necessity for characterization techniques of nanodomains with increasing activities in developing new nanomaterials.

APPENDIX

MATLAB Programming

Plotting of trajectories and calculation of mean square displacement as a function of time, angles between successive steps is given.

For single trajectories in single .txt file

```
clear all
clc

format long
first_part=sprintf('%s','Results_17412');
input_file=sprintf('%s%s',first_part,'.txt');
outfile1=sprintf('%s%s',first_part,'_MSD','_o.txt');
outfile_jpg1=sprintf('%s%s',first_part,'_All','_jpg');
outfile2=sprintf('%s%s',first_part,'_Angle','_o.txt');
outfile3=sprintf('%s%s',first_part,'_Traj','_o.txt');
matrix_read=load(input_file);
xx = [matrix_read(:,2)']*0.08889; % for pixel size=0.08889um
yy = [matrix_read(:,3)']*0.08889; % for pixel size=0.08889um
delta_r_2=[];
delta_t=0.1;
MSD=[];
T=[];
```

```
t=0;
for jj=1:(length(xx)-1);
   for ii=(jj+1):length(xx)
      a=xx(ii)-xx(ii-jj);
      b=yy(ii)-yy(ii-jj);
      dr_2=a^2+b^2;
      delta_r_2=[delta_r_2 dr_2];
   end
   MSD=[MSD sum(delta_r_2)/length(delta_r_2)];
   delta_r_2=[];
end;


MSD_sub=MSD(1:(length(MSD)/2));


for jj=1:(length(xx)-2)
   mag_A=sqrt((xx(jj+1)-xx(jj))^2+(yy(jj+1)-yy(jj))^2);
   mag_B=sqrt((xx(jj+2)-xx(jj+1))^2+(yy(jj+2)-yy(jj+1))^2);
   angle_v(jj)=acos( ( (xx(jj+1)-xx(jj))*(xx(jj+2)-xx(jj+1))+...
   (yy(jj+1)-yy(jj))*(yy(jj+2)-yy(jj+1)) ) / (mag_A*mag_B) ) / pi ;
end;


[n, xout]=hist(angle_v);
ANGLE=zeros(length(n),2);
ANGLE(:,2)=n;
ANGLE(:,1)=xout;
```

```
MSD2=zeros(length(MSD_sub),2);
MSD2(:,2)=MSD_sub(1:length(MSD_sub));


for ii=1:length(MSD_sub);
   MSD2(ii,1)=ii*delta_t;
end;


Traj(:,1)=[matrix_read(:,3)'];
Traj(:,2)=[matrix_read(:,2)'];


subplot(1,3,1)
plot(xx,yy,'-o')
title('Trajectory of the particle');
xlabel('x (um)')
ylabel('y (um)')
subplot(1,3,2)
plot(MSD_sub,'-*')
title('MSD vs Time for all steps')
xlabel('time (s)')
ylabel('MSD (um^2)')
subplot(1,3,3)
hist(angle_v);
title('Histogram of angles between each steps')
xlabel('angle')
ylabel('occurance')
saveas(gcf,outfile_jpg1,'jpg');
```

```
save(outfile1,'MSD2','-ASCII','-TABS');
save(outfile2,'ANGLE','-ASCII','-TABS');
save(outfile3,'Traj','-ASCII','-TABS');
```

For multiple trajectories in single .txt file

```
clear all
clc
close all;

format long
first_part=sprintf('%s','Results_2-4-6_hours');
input_file=sprintf('%s%s',first_part,'.txt');
matrix_read_all=load(input_file);
a=matrix_read_all(:,1)
zeros_vector_s=a(1:(length(a)-1))-a(2:length(a))
zeros_vector=find(zeros_vector_s~=-1)
delta_r_2=[];
delta_t=0.1;

for kk=1:(length(zeros_vector)-1);
    matrix_read=matrix_read_all((zeros_vector(kk)+1):zeros_vector(kk+1),:);
    outfile=sprintf('%s%i%s',first_part,kk,'_MSD2','_o.txt');
    outfile2=sprintf('%s%i%s',first_part,kk,'_Angle','_o.txt');
    outfile_jpg=sprintf('%s%i%s',first_part,kk,'_jpg');
    yy = [matrix_read(:,2)']*0.08889; % for pixel size=0.08889um
    xx = [matrix_read(:,3)']*0.08889; % for pixel size=0.08889um
```

```
aa=xx;
MSD=[];
T=[];
t=0;
for jj=1:(length(xx)-1);
   for ii=(jj+1):length(xx);
      a=xx(ii)-xx(ii-jj);
      b=yy(ii)-yy(ii-jj);
      dr_2=a^2+b^2;
      delta_r_2=[delta_r_2 dr_2];
   end
   MSD=[MSD sum(delta_r_2)/length(delta_r_2)];
   delta_r_2=[];
end;


MSD_sub=MSD(1:(length(MSD)/4));


for ss=1:(length(aa)-2);
mag_A=sqrt((xx(ss+1)-xx(ss))^2+(yy(ss+1)-yy(ss))^2);
mag_B=sqrt((xx(ss+2)-xx(ss+1))^2+(yy(ss+2)-yy(ss+1))^2);
angle_v(ss)=acos( ( (xx(ss+1)-xx(ss))*(xx(ss+2)-xx(ss+1))+...
(yy(ss+1)-yy(ss))*(yy(ss+2)-yy(ss+1)) ) / (mag_A*mag_B) ) / pi ;
end;
%    angle_v'
[n, xout]=hist(angle_v);
ANGLE=zeros(length(n),2);
```

```
ANGLE(:,1)=xout;
ANGLE(:,2)=n;


MSD2=zeros(length(MSD_sub),2);
MSD2(:,2)=MSD_sub(1:length(MSD_sub));


for ff=1:length(MSD_sub);
   MSD2(ff,1)=ff*delta_t;
end;


x0 = mean(MSD2(:,1)); y0 = mean(MSD2(:,2))
[u,s,v] = svd([MSD2(:,1)-x0,MSD2(:,2)-y0],0);
md = max(sqrt((MSD2(:,1)-x0).^2+(MSD2(:,2)-y0).^2));
tink = linspace(-md,md);
X = x0+v(1,1)*tink;
Y = y0+v(2,1)*tink;
slope=v(2,1)/v(1,1);
diffcoef=slope/2; % diffcoef=slope/4; for 2D diffusion coefficients
aka=sprintf('Linear Fit \n Diffusion coefficient for 1D is = %f um^2/sec.',diffcoef);


subplot(2,2,1)
plot(xx,yy,'-o')
title('Trajectory of the particle');
xlabel('x (um)')
ylabel('y (um)')
axis ij
```

```
    axis equal

    subplot(2,2,2)
    hist(angle_v);
    title('Histogram of angles between each steps')
    xlabel('Angle')
    ylabel('Occurance')

    subplot(2,2,3)
    plot(MSD2(:,1),MSD2(:,2),'-*')
    title('MSD vs Time for one step')
    xlabel('time (s)')
    ylabel('MSD(um^2)')

    subplot(2,2,4)
    plot(X,Y,'r-',MSD2(:,1),MSD2(:,2),'b-',x0,y0,'go')
    title(aka);
    xlabel('time (s)')
    ylabel('MSD (um^2)')
    saveas(gcf,outfile_jpg,'jpg');
    save(outfile,'MSD2','-ASCII','-TABS');
    save(outfile2,'ANGLE','-ASCII','-TABS');

angle_v=[];
end;
```

BIBLIOGRAPHY

[1] G. J. Schütz, V. Ph. Pastushenko, H. J. Gruber, H.-G. Knaus, B. Pragl and H. Schindler, 3D Imaging of Individual Ion Channels in Live Cells at 40 nm Resolution, Single Mol., Vol.1, 25-31, (2000).

[2] W. E. Moerner, A Dozen Years of Single-Molecule Spectroscopy in Physics, Chemistry, and Biophysics, J. Phys. Chem. B, Vol.106, 910-927, (2002).

[3] G. Seisenberger, M. U. Ried, T. Endress, H. Büning, M. Hallek and C. Brauchle, Real-Time Single-Molecule Imaging of the Infection Pathway of an Adeno-Associated Virus, Science, Vol.294, 1929-1932, (2001).

[4] A. Yildiz, J. N. Forkey, S. A. McKinney, T. Ha, Y. E. Goldman and P. R. Selvin, Myosin V Walks Hand-Over-Hand: Single Fluorophore Imaging with 1.5-nm Localization, Science, Vol.300, 2061-2065, (2003).

[5] K. Shiroguchi and K. Kinosita Jr., Myosin V Walks by Lever Action and Brownian Motion, Science, Vol.316, 1208-1212, (2007).

[6] S. Wieser and G. J. Schütz, Tracking single molecules in the live cell plasma membrane-Do's and Don't's, Methods, Vol.46, 131-140, (2008).

[7] Y. Fu, F. Ye, W. G. Sanders, M. M. Collinson and D. A. Higgins, Single Molecule Spectroscopy Studies of Diffusion in Mesoporous Silica Thin Films, J. Phys. Chem. B, Vol.110, 9164-9170, (2006).

[8] C. Seebacher, C. Hellriegel, C. Bräuchle, M. Ganschow and D. Wöhrle, Orientational Behavior of Single Molecules in Molecular Sieves: A Study of Oxazine Dyes in $AlPO_4$-5 Crystals, J. Phys. Chem. B, Vol.107, No.23, 5445-5452, (2003).

[9] C. Hellriegel, J. Kirstein, C. Brauchle, V. Latour, T. Pigot, R. Olivier, S. Lacombe, R. Brown, V. Guieu, C. Payrastre, A. Izquierdo and P. Mocho, Diffusion of Single Streptocyanine Molecules in the Nanoporous Network of Sol-Gel Glasses, J. Phys. Chem. B, Vol.108, 14699-14709, (2004).

[10] C. A. Werley and W. E. Moerner, Single-Molecule Nanopores Explore Defects in Spin-Grown Crystals, J. Phys. Chem. B, Vol.110, 18939-18944, (2006).

[11] K. S. McCain, D. C. Hanley and J. M. Harris, Single Molecule Fluorescence Trajectories for Investigating Molecular Transport in Thin Silica Sol-Gel Films, Anal. Chem., Vol.75, 4351-4359, (2003).

[12] A. Zumbusch, L. Fleury, R. Brown, J. Bernard and M. Orrit, Probing Individual Two-Level Systems in a Polymer by Correlation of Single Molecule Fluorescence, Phys. Rev. Lett., Vol. 70, No.23, 3584-3587, (1993).

[13] M. B. J. Roeffaers, B. F. Sels, H. Uji-i, F. C. de Schryver, P. A. Jacobs, D. E. de Vos and J. Hofkens, Spatially Resolved Observation of Crystal-Face Dependent Catalysis by Single Turnover Counting, Nature, Vol.439, 572-575, (2006).

[14] M. Orrit and J. Bernard, Single Pentacene Molecules Detected by Fluorescence Excitation in a p-Terphenyl Crystal, Phys. Rev. Lett., Vol.65, No.21, 2716–2719, (1990).

[15] X. S. Xie, Single-Molecule Spectroscopy and Dynamics at Room Temperature, Acc. Chem. Res., Vol. 29, No.12, 598-606, (1996).

[16] M. Orrit, Single-Molecule Spectroscopy: The Road Ahead, J. Chem. Phys., Vol.117, No.24, 10938-10946, (2002).

[17] W. E. Moerner and D. P. Fromm, Methods of Single-Molecule Fluorescence Spectroscopy and Microscopy, Rev. Sci. Instrum., Vol.74, No.8, 3597-3617, (2003).

[18] D. Majolino, C. Corsaro, V. Crupi, V. Venuti and U. Wanderlingh, Water Diffusion in Nanoporous Glass: An NMR Study at Different Hydration Levels, J. Phys. Chem. B, Vol.112, 3927-3930, (2008).

[19] G. Buntkowsky, H. Breitzke, A. Adamczyk, F. Roelofs, T. Emmler, E. Gedat, B. Grünberg, Y. Xu, H. Limbach, I. Shenderovich, A. Vyalikh and G. Findenegg, Structural and Dynamical Properties of Guest Molecules Confined in Mesoporous Silica Materials Revealed by NMR, Phys. Chem. Chem. Phys., Vol.9, 4843-4853, (2007).

[20] V. Kukla, J. Kornatowski, D. Demuth, I. Girnus, H. Pfeifer, L. V. C. Rees, S. Schunk, K. K. Unger and J. Karger, NMR Studies of Single-File Diffusion in Unidimensional Channel Zeolites, Science, Vol.272, 702–704, (1996).

[21] M. J. Wirth, D. J. Swinton and M. D. Ludes, Adsorption and Diffusion of Single Molecules at Chromatographic Interfaces, J. Phys. Chem. B, Vol.107, 6258-6268, (2003).

[22] S. Rols, H. Jobic and H. Schober, Monitoring Molecular Motion in Nano-Porous Solids, C. R. Physique, Vol.8, 777-788, (2007).

[23] W. E. Moerner, New Directions in Single-Molecule Imaging and Analysis, PNAS, Vol.104, No.31, 12596-12602, (2007).

[24] F. Kulzer and M. Orrit, Single-Molecule Optics, Ann. Rev. Phys. Chem., Vol.55, 585-611, (2004).

[25] Ph. Tamarat, A. Maali, B. Lounis and M. Orrit, Ten Years of Single Molecule Spectroscopy, J. Phys. Chem. A, Vol.104, No.1, 1-16, (2000).

[26] H. Qian, M. Sheetz, E. Elson, Single Particle Tracking. Analysis of Diffusion and Flow in Two-Dimensional Systems, Biophys. J., Vol.60, No.4, 910-921, (1991).

[27] Th. Schmidt, G. J. Schütz, W. Baumgartner, H. J. Gruber and H. Schindler, Imaging of Single Molecule Diffusion, Proc. Natl. Acad. Sci. USA, Vol.93, 2926-2929, (1996).

[28] B. Sick, B. Hecht, U. P. Wild and L. Novotny, Probing confined fields with single molecules and vice versa, Journal of Microscopy, Vol. 202, 365-373, (2000).

[29] C. Jung, C. Hellriegel, J. Michaelis and C. Bräuchle, Single-Molecule Traffic in Mesoporous Materials: Translational, Orientational, and Spectral Dynamics, Adv. Mater., Vol.19, No.7, 956–960, (2007).

[30] C. Jung, C. Hellriegel, B. Platschek, D. Wöhrle, T. Bein, J. Michaelis and C. Bräuchle, Simultaneous Measurement of Orientational and Spectral Dynamics of Single Molecules in Nanostructured Host-Guest Materials, J. Am. Chem. Soc., Vol.129, 5570–5579, (2007).

[31] C. Jung, J. Kirstein, B. Platschek, T. Bein, M. Budde, I. Frank, K. Müllen, J. Michaelis and C. Brauchle, Diffusion of Oriented Single Molecule with Switchable Mobility in Networks of Long Unidimensional Nanochannels, J. Am. Chem. Soc., Vol.130, 1638-1648, (2008).

[32]R. E. Thompson, D. R. Larson, and W. W. Webb, Precise Nanometer Localization Analysis for Individual Fluorescent Probes, Biophys. J. Vol.82, 2775-2783 (2002).

[33] A. Zürner, J. Kirstein, M. Döblinger, C. Brauchle and T. Bein, Visualizing Single-Molecule Diffusion in Mesoporous Materials, Nature, Vol.450, 705-708, (2007).

[34] J. Kirstein, B. Platschek, C. Jung, R. Brown, T. Bein and C. Brauchle, Exploration of Nanostructured Channel Systems with Single-Molecule Probes, Nature Materials, Vol.6, 303-310, (2007).

[35] P. S. Burada, P. Hanggi, F. Marchesoni, G. Schmid and P. Talkner, Diffusion in Confined Geometries, ChemPhysChem, Vol.10, 45-54, (2009).

[36] H. Yang, Y. Liu, H. Zhang and Z. Li, Diffusion of single alkane molecule in carbon nanotube studied by molecular dynamics simulation, Polymer, Vol.47, 7607-7610, (2006).

[37] J. Caro, F. Marlow and M. Wübbenhorst, Chromophore-Zeolite Composites: The Organizing Role of Molecular Sieves, Adv. Mater., Vol.6, No.5, 413-416, (1994).

[38] A. L. Demirel, H. Schlaad, Controlling the morphology of polybutadiene-poly(ethylene oxide) diblock copolymers in bulk and the orientation in thin films by attachment of alkyl side chains, Polymer, Vol.49, 3470-3476, (2008).

[39] J. L. Meinershagen and T. Bein, Optical Sensing in Nanopores. Encapsulation of the Solvatochromic Dye Nile Red in Zeolites, J. Am. Chem. Soc., Vol.121, 448-449, (1999).

[40] P. Yang, G. Wirnsberger, H. C. Huang, S. R. Cordero, M. D. McGehee, B. Scott, T. Deng, G. M. Whitesides, B. F. Chmelka, S. K. Buratto and G. D. Stucky, Mirrorless Lasing from Mesostructured Waveguides Patterned by Soft Lithography, Science, Vol.287, 465-467, (2000).

[41] C. Zander, J. Enderlein and R. A. Keller, Single Molecule Detection in Solution, Wiley-VCH, (2002)

[42] J. U. Kirstein, Diffusion of Single Molecules in Nanoporous Mesostructured Materials, Ph.D. thesis, Ludwig Maximilians University, 2007.

[43] K. A. Willets, O. Ostroverkhova, S. Hess and M. He, Novel Fluorophores for Single-Molecule Imaging, Proc. SPIE, 522 (2003).

[44] Michel Orrit, Single Molecule Optics, 2004.

[45] W. E. Moerner and L. Kador, Optical Detection and Spectroscopy of Single Molecules in a Solid, Phys. Rev. Lett., Vol.62, No.21, 2535–2538, (1989).

[46] J. C. Schweizer, Practical Course: Single-Particle-Tracking, Biophysics-Schwille Lab, 2007.

[47] www.sensorcleaning.com/whatisasensor.php

[48] F. Kulzer, F. Koberling, T. Christ, A. Mews and Th. Basche, Terrylene in p-terphenyl: Single Molecule Experiments at Room Temperature, Chem. Phys. Vol.247, 23-34, (1999).

[49] U. Kubitscheck, O. Kückmann, T. Kues and R. Peters, Imaging and Tracking of Single GFP Molecules in Solution, Biophys. J., Vol.78, 2170-2179, (2000).

[50] https://weeman.inf.ethz.ch/ParticleTracker/

[51] http://rsbweb.nih.gov/ij/

[52] I. F. Sbalzarini and P. Koumoutsakos, Feature point tracking and trajectory analysis for video imaging in cell biology, J. Struct. Biol. Vol.151, No.2, 182-195, (2005).

LIST OF PUBLICATIONS

Published Work

1)   M. Yorulmaz, A. Kiraz, and A. L. Demirel. "Motion of Single Terrylene Molecules in Confined Channels of Poly(butadiene)-Poly(ethylene oxide) Diblock Copolymer" J. Phys. Chem. B 113 (29), 9640-9643 (2009).

2)   A. Kiraz, S. C. Yorulmaz, M. Yorulmaz, and A. Sennaroglu. "Raman Lasing near 650 nm from Pure Water Microdroplets on a Superhydrophobic Surface" Photon. Nanostruct.: Fundam. Appl. (2009). (accepted for publication)

Contributions to Conferences and Meetings

3)   M. Yorulmaz, A. Kiraz and A. L. Demirel, "Single Molecule Tracing to Analyze the Surface Morphology of Block-Copolymer Thin Films," DPG Spring Meeting, Dresden (22 27 March 2009) (International - Oral Presentation).

4)   M. Yorulmaz, A. Kiraz and A. L. Demirel, "Blok Kopolimerler ile Oluşturulan Çevrelenmiş Geometrilerde Tek Moleküllerin İzlenmesi ," 10. Ulusal Optik, Elektro-Optik ve Fotonik Çalışma Toplantısı, Kocaeli Üniversitesi, Kocaeli (17 Ekim 2008) (National - Poster Presentation).

5)   M. Yorulmaz, A. Kiraz and A. L. Demirel, "Single Molecule Imaging to Analyze Diffusion and Dipole Orientation," MediNano, Istanbul (6 - 7 October 2008) (International - Poster Presentation).

6) M. Yorulmaz, A. Kiraz and A. L. Demirel, "Single Molecule Tracing in Confined Geometries," 3rd Bilateral Workshop of KU-MPI-CPFS on "Novel Materials," Istanbul (19-20 May 2008) (International - Oral Presentation).

7) M. Yorulmaz, A. Kiraz and A. L. Demirel, "Tek Molekül Görüntülemesi Yöntemi ile Moleküllerin Yayınımı ve Dipol Yönelimlerinin İncelenmesi," 9. Ulusal Fotonik Çalıştayı (FOTONIK 2007), Aselsan, Ankara (28 Eylül 2007) (National - Poster Presentation).

8) M. Yorulmaz, A. Kiraz and A. L. Demirel, "Single Molecule Imaging to Analyze Diffusion and Dipole Orientation," PhOREMOST 'ADVANCES IN NANOPHOTONICS' Workshop, Istanbul (13-15 September 2007) (International - Poster Presentation).

VITA

Mustafa Yorulmaz completed the high school in Selçuklu Anadolu Lisesi, Konya, Turkey in 2002. He received his B. Sc. degree in Physics from Bilkent University, Ankara, Turkey in 2007. He joined Materials Science and Engineering program at Koç University in 2007. He received his M. Sc. degree from Koç University in 2009. His master thesis work was titled as "Single Molecule Tracking in Confined Geometries". He will start his Ph. D. degree at Leiden University in the Netherlands working on "Single-Molecule Studies of Soft Matter". He is a student member of Optical Society of America (OSA).